International Journal of Greenhouse Gas Control 22 (2014) 123–138

Contents lists available at ScienceDirect

International Journal of Greenhouse Gas Control

journal homepage: www.elsevier.com/locate/ijggc

Model complexity in carbon sequestration: A design of experiment and response surface uncertainty analysis

Shuiquan Li[a,*], Ye Zhang[b,*]

[a] Enhanced Oil Recovery Institute, University of Wyoming, 1000 E. University Ave., Laramie, WY 82071, USA
[b] Department of Geology & Geophysics, University of Wyoming, 1000 E. University Ave., Laramie, WY 82071, USA

ARTICLE INFO

Article history:
Received 12 July 2013
Received in revised form
10 December 2013
Accepted 13 December 2013

Keywords:
Carbon sequestration
Geologic reservoir modeling
Uncertainty analysis
Design of experiment
Response surface
Proxy model

ABSTRACT

Geologic carbon sequestration (GCS) is considered a promising means of reducing atmospheric carbon dioxide (CO_2). In Wyoming, GCS is proposed for the Nugget Sandstone in Moxa Arch, a deep, regional-scale saline aquifer with a large CO_2 storage potential. For a proposed storage site, this study builds a suite of increasingly complex conceptual geologic model families, using subsets of the site characterization data: a homogeneous model family (FAM1), a stationary petrophysical model family (FAM2), a stationary facies model family with sub-facies petrophysical variability (FAM3), and a non-stationary facies model family (with sub-facies variability) conditioned to soft data (FAM4). These families, representing alternative conceptual site models built with increasing data, were simulated with the same CO_2 injection test (50 years at 1/10 Mt (1.0×108 kg) per year), followed by 2950 years of monitoring. Using the design of experiment, an efficient sensitivity analysis (SA) is conducted for all families, systematically varying uncertain aquifer parameters, while assuming identical well configuration, injection rate, bottomhole pressure constraint, and boundary conditions, i.e., the model is considered a part of a larger, semi-infinite system, where both the injected CO_2 and the formation brine can flow out. The SA results are compared among the families to identify parameters that have 1st order impact on predicting CO_2 storage ratio (SR) at two different time scales, i.e., end of injection and end of monitoring. This comparison indicates that, for this deep aquifer with a gentle incline, geologic modeling factors do not significantly influence the short-term prediction of the CO_2 storage ratio. However, these factors become more important over the monitoring time, but only for those families where such factors are accounted for (in other words, their long-term importance cannot be revealed by the relatively simple conceptual models). Based on the SA results, a response surface analysis is conducted to generate prediction envelopes of the storage ratio, which are also compared among the families, and at both time scales. Results suggest a large uncertainty in the predicted storage ratio, given the uncertainties in model parameters and modeling choices: the SR varies from 5–60% (end of injection) to 18–100% (end of monitoring), although its variation among the model families due to different modeling choices is relatively minor. Moreover, long-term leakage risk is considered small at the proposed site. This is because, in the lowest-SR scenarios, all model families predict gravity-stable supercritical CO_2 migrating toward the bottom of the aquifer. In the highest-SR scenarios, supercritical CO_2 footprints are relatively insignificant by the end of monitoring.

Published by Elsevier Ltd.

1. Introduction

Geological carbon sequestration (GCS) is considered to be a promising option for mitigating global climate change (IPCC, 2013). Wyoming produces approximately 40% of the coal in the United States. In 2000, coal-fired power plants in the state emitted a total of 51 million tons (Mt) of CO_2 into the atmosphere (Stauffer et al., 2009a). By 2009, the emission rate had risen to 54.4 Mt/year and it is further projected to increase with new energy demand (Deng et al., 2012; Easley et al., 2013). To achieve climate mitigation, power plants such as these are the chief targets for conversion to allow the capture of CO_2 and subsequent sequestration underground. Given the magnitude of the emission rate, CO_2 needs to be sequestered at industrial scales for which deep saline aquifers with large storage capacity are needed (Bachu, 2000). The Moxa Arch anticline in western Wyoming is a deeply buried subsurface structure and a proposed GCS site (Fig. 1). Multiple deep saline aquifers with large storage capacities have been identified that lie adjacent to several coal-fired power plants including the 2.1 GW Jim Bridger Power Plant (Li et al., 2011). The anticline consists of geologic formations ranging from Precambrian crystalline rocks to Holocene alluvial sands and gravels. It hosts natural gas in the Frontier Sandstone

* Corresponding authors. Tel.: +1 307 766 7381.
E-mail addresses: sli2@uwyo.edu (S. Li), yzhang9@uwyo.edu (Y. Zhang).

1750-5836/$ – see front matter. Published by Elsevier Ltd.
http://dx.doi.org/10.1016/j.ijggc.2013.12.007

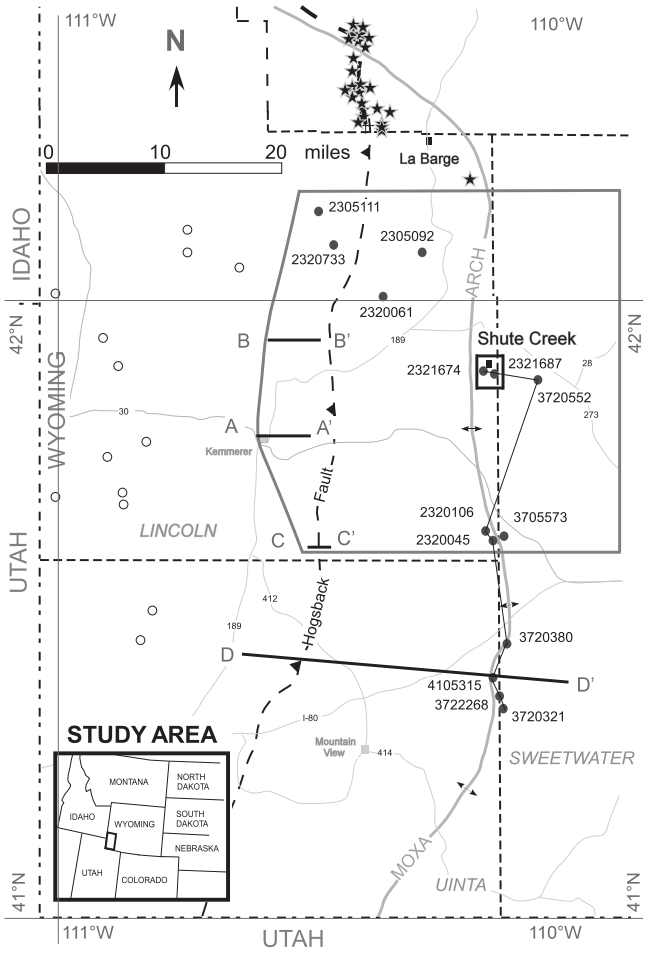

Fig. 1. A map of the study site with the location of a regional model indicated by the larger outline. Wells that penetrate to the depth of the Nugget Sandstone are shown: solid symbols denote wells inside Moxa Arch (circles with API numbers were used in well log correlation to create the regional model (Li et al., 2011); stars denote wells from natural gas fields northwest of La Barge where Nugget facies and petrophysical properties were examined); empty circles are those that lie outside the Arch where Nugget facies and petrophysical properties were examined. AA′, BB′, CC′, and DD′ are cross sections used in creating the regional model, from which a section model centered at Shute Creek (small box) is extracted for CO_2 simulation. Also shown is a thin line connecting a set of wells, which extends from Shute Creek toward the southern Moxa Arch. Along this line, a well log correlation profile is presented in Fig. 2.

(Harstad et al., 1996) and natural CO_2 in the Madison Limestone (Huang et al., 2011), attesting to the sealing capacity of multiple, low-permeability caprock formations. At the Shute Creek gas plant (Fig. 1), acid gas disposal into the Madison Limestone has been ongoing since 2005 at a rate of 60 MMscf/day (1.7 MM m^3/day), and is one of the world's largest acid gas reinjection projects (Huang et al., 2011). In the region surrounding the gas plant, few wells perforate these deep formations, reducing leakage risk via wellbores. Interpretation of three-dimensional seismic data acquired northwest of Shute Creek has not identified large faults, suggesting structure continuity. With infrastructure including deep injection wells and CO_2 pipelines, the gas plant is considered a candidate site for CO_2 injection.

In evaluating a GCS site, reservoir flow simulation is commonly performed based on a geologic site model which characterizes subsurface structure, facies, and other heterogeneities. To resolve detailed heterogeneity, increasing subsurface characterization effort is required, and the greater the detail, the higher the cost. GCS, in particular, CO_2 storage in deep saline aquifers, is frequently considered a "cost center". Moreover, for the type, amount, and accessibility of data at a given site, different geologic models can be built, ranging from the simple to complex. For example, petrophysical properties can be alternatively modeled assuming homogeneity (Birkholzer and Zhou, 2009) or heterogeneity (Deng et al., 2012), the latter requiring advanced modeling techniques supported by additional data. Although such data can be obtained from drilling and logging the aquifer, or from high-resolution geophysical surveys, extensive data acquisition is not realistic at large scales where industrial CO_2 storage is concerned. Besides the cost constraint, leakage from wellbores must be minimized, limiting the number of boreholes that can be drilled. A critical issue in GCS is therefore to determine the right types of data to collect, and, based on these data, the right type of geologic model to construct, leading to a cost-effective strategy in data collection. Such models, as input to flow simulation, will ideally lead to adequate, or sufficiently accurate, predictions of the desired outcomes, while models are not overly detailed and are therefore cost-prohibitive to construct. However, the identification of an optimal model is challenging due to the fact that in GCS modeling, a variety of uncertainty factors exist, including geologic factors influencing reservoir porosity and permeability, engineering factors influencing gas trapping and migration, and environmental factors influencing CO_2 fluid properties. Although the uncertainty factors that exert the most significant impact on CO_2 predictions are of the most interest—these are the ones that need to be better characterized, reducing their uncertainties and therefore uncertainty in predictions, as model complexity (level of detail) increases, more geologic uncertainty factors can come into play (Friedmann et al., 2003; Milliken et al., 2007).

Toward the overall objective of developing cost-effective models, this study aims to understand model complexity in GCS and the associated data needs, including both static and dynamic data. For the storage formation, the Nugget Sandstone in Moxa Arch has been chosen, which is a deep (13,000–17,000 ft depth), regional-scale saline aquifer with a large storage potential, due to its large areal extent, significant thickness (on average, 700 ft (213 m) thick), and relatively high porosity. It is separated from the overlying gas-bearing Frontier Sandstone by multiple, low-permeability formations, while Frontier itself is capped by low-permeability cap rocks. Detailed discussion of the Nugget Sandstone's geological and depositional settings can be found in Li et al. (2011). Along a profile connecting several wells (Fig. 1), well log correlation suggests the continuity of the Nugget Sandstone at regional scales (Fig. 2), which is confirmed by seismic line shots in southern Moxa Arch (David et al., 1975; Royse et al., 1975). At the Shute Creek gas plant, Nugget Sandstone overlies the Madison Limestone, where acid gas injection is ongoing. Here, few wells perforate to the depth of the Nugget (Fig. 1), minimizing leakage risk. The gas plant, where existing wells can be fitted for injecting CO_2, is a proposed GCS site. However, due to limited well data at the plant, much uncertainty exists in describing Nugget Sandstone's porosity and permeability. On the one hand, reservoir heterogeneity is known to exist as evidenced by examining the wireline logs and computed clay volumes of formation (Fig. 2). On the other hand, large distances between wells give rise to uncertainty as to the appropriate geologic modeling method that can best capture the relevant heterogeneity. In fact, alternative modeling methods exist, whereas the effect of different methods on porosity/permeability prediction, and therefore CO_2 storage modeling, is unknown.

To understand the uncertainty in CO_2 storage modeling in the Nugget Sandstone and the impact of model complexity on CO_2 predictions, this study creates multiple families of geologic models with different techniques to determine if the list of "heavy hitters" (i.e., uncertainty factors whose variations have significant impact on a prediction outcome) will change with the modeling choice. Because CO_2 flow is often dominated by viscous force during injection and gravity force during monitoring, the list of heavy hitters

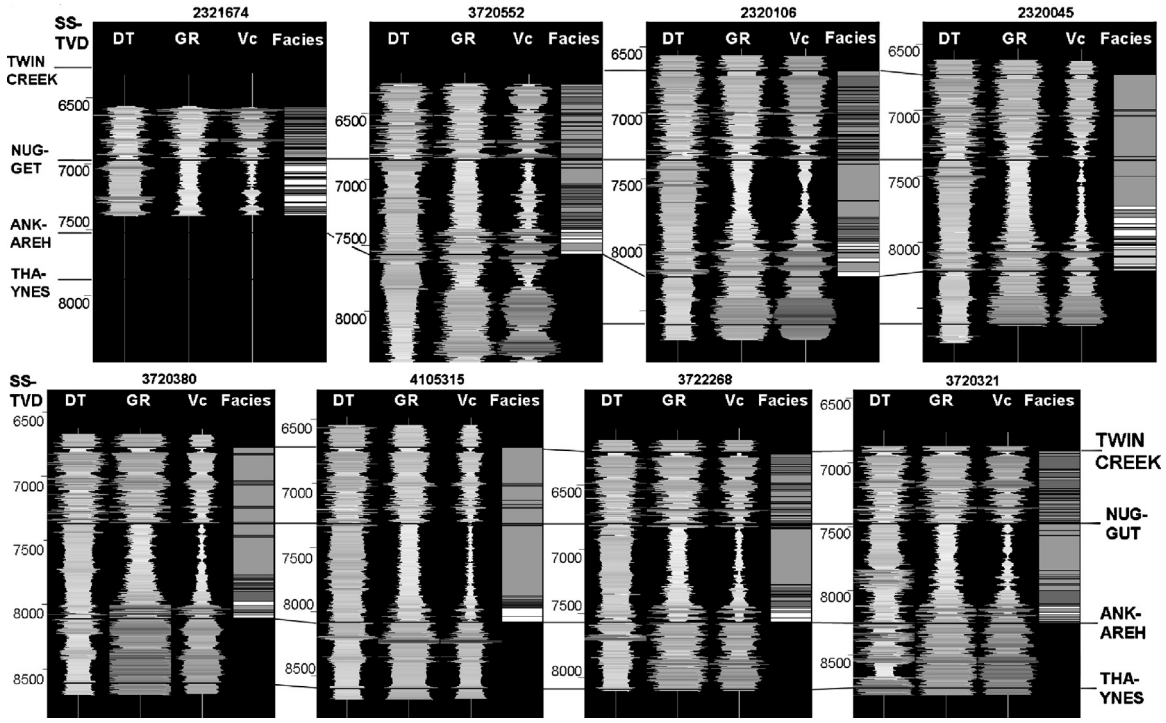

Fig. 2. Formation structure correlation for the Nugget Sandstone along the north-south-oriented line in Fig. 1. Well API is shown at the top of each subplot. The top panel consists of wells inside the regional model; the bottom panel continues from the top panel and consists of wells south of the regional model. The top of the Nugget Sandstone is denoted by "Nugget" which is set as the baseline for correlation; the bottom is denoted by "Ankareh", an underlying formation. SSTVD = subsea true vertical depth; DT = sonic logs; GR = gamma ray; *Vc* = computed formation clay volume; Facies = inferred petrofacies from wireline logs (Li et al., 2011).

influencing its predictions may change over time, as well as the uncertainty in the predictions. The uncertainty outcome will therefore be evaluated at two time scales, i.e., end of injection, and end of monitoring. Furthermore, because computational challenge in carrying out a full uncertainty analysis with a large reservoir model can be significant, the efficient design of experiment (DoE) and response surface (RS) methodology is adopted for analyzing the parameter importance and prediction uncertainty. In the following, an overview of the DoE methodology is introduced, followed by a presentation of the study method. Results are discussed and summarized, leading to a set of conclusions and insights.

2. Overview of the DoE methodology

In subsurface modeling, uncertainty analysis is usually initiated with a parameter sensitivity analysis (SA). Traditionally, SA is conducted one parameter at a time to evaluate sensitivity of model outcomes in response to parameter variation. For each parameter varied, 3 values are typically defined (e.g., P10, P50, P90), which reflect a prior assessment of parameter uncertainty. A "base-case" simulation is defined, by all parameters assuming their P50 values. In the SA, a parameter is first set at its P10 level, and then its P90 level, while all other parameters are kept at P50 levels. (Given N parameters, 2N + 1 simulations are needed.) Tornado diagrams can then be generated to rank the effect of each parameter on a prediction outcome, although this ranking can be biased because the SA runs are not fully exploring the parameter space, e.g., combinations at the parameter space boundary are not evaluated. The SA also assumes that parameters varied are independent of one another, although in reality parameters are often correlated. To understand the prediction uncertainty arising out of parameter uncertainty, Monte Carlo (MC) simulation can be used, whereas uncertainty of an outcome is estimated by assuming probability density functions (*pdfs*) for the uncertain parameters. Input parameters are randomly drawn from these *pdfs*, as input to full-physics reservoir simulation. Statistical distribution of an outcome is then evaluated by repeated random draws and thus repeated simulations. This method, though conceptually straightforward, is computationally intensive, as often hundreds, if not thousands, of reservoir simulations are needed to sample the parameter space. This becomes an issue for large models running long simulation times. Although Latin hypercube MC sampling has been explored as a more efficient alternative to brute force MC (Stauffer et al., 2009b), such analysis still requires a large number of model runs that become prohibitive when model size is large. One way to overcome this difficulty is to develop a computationally efficient proxy (or surrogate) model for the reservoir simulator. The design of experiment (DoE) methodology is a promising tool in reservoir analysis. DoE can fully explore the parameter space, is computationally efficient, and does not assume parameter independence. Its results can be used to create a response surface (RS) model, which is an analytic function that can be quickly evaluated for any performance outcome given any parameter combinations. After suitable verification, the RS model becomes a proxy model for reservoir simulation with which a MC analysis can be conducted to evaluate uncertainty in predictions. This analysis is orders of magnitude faster than brute force MC with full-physics simulations. Below, DoE and RS methods are introduced with greater detail.

In DoE, the SA is conducted by varying a subset of the uncertain input parameters simultaneously according to a design table (Montgomery, 2008). The parameters varied (also referred to as factors) can be continuous or categorical, the latter often reflecting modeling choices. Results of the SA are examined with multivariate analysis of variance (MANOVA), which identifies the parameters that exert statistically significant effects on a simulation outcome. Though a variety of designs are available (the same design can be used for analyzing multiple outcomes), a two-level Plackett–Burman (PB) design is adopted here. Compared to other designs, the PB design is the most parsimonious for selecting a parameter subset for simulations, providing large savings in

program execution time. However, this design can only identify the main effects and confound interactions with the main effects. It is most useful as a screening tool to identify the most significant uncertainty factors with the fewest number of simulation runs. For example, in scoping studies to guide early data collection, PB design alone can be used (Jian et al., 2002; Milliken et al., 2007; Choi et al., 2007), while PB combined with a RS design is effective in analyzing a variety of reservoir performance outcomes (Friedmann et al., 2003; Meddaugh et al., 2004; Yeten et al., 2005).

The RS analysis consists of fitting an analytical function to a simulation outcome (Myers and Montgomery, 1995). This function is generated by running reservoir simulations according to a RS design, using factors that have been previously identified by the screening (PB) design as the most important for predicting that outcome at a user-specified significance level. Factors that have been identified as insignificant are removed. In the RS design, three values for each factor are necessary, i.e., −/0/+ (low/medium/high), which can correspond to key probabilities, although this is not a requirement. To generate the RS function, a quadratic polynomial is fitted to the simulation outcomes via multilinear regression. Though alternative fitting methods exist (e.g., kriging, splines, neural net), quadratic polynomial is found accurate and robust in analyzing a variety of reservoir problems (Wang and White, 2002; Peng and Gupta, 2004; Yeten et al., 2005). Many RS designs are available (e.g., space filling, fractional factorial, D-optimal, etc.), although the "best" design is often problem dependent. Researchers rely on verification to test the robustness of a chosen design in replicating simulated values at non-design points. In this study, a customized fractional factorial design is used. Results are verified at the PB design points, which lie on the parameter space boundary. According to Peng and Gupta (2004), these "extreme test runs" can exaggerate the RS errors, although this decision can lead to significant computational savings. After the verification, the RS model is considered a proxy for reservoir simulation, i.e., a statistically based predictive model between the important input factors and the simulation outcome (response).

With the RS model, a MC analysis is run by randomly drawing the factors according to their respective *pdfs*, which leads to a *pdf* of the outcome. Two points must be noted: (1) ranges of the factors drawn cannot go beyond the ranges in which the RS model is developed and verified. (2) If strong correlations exist among the factors, joint *pdfs* should ideally be developed. However, for sites with sparse data, it is challenging to develop joint *pdfs*, while research evaluating the effect of independent sampling on inducing RS errors is ongoing. In this study, a non-informative, uniform distribution is assigned to the uncertain input factors, including continuous and categorical variables, because information pertaining to their exact *pdfs* is lacking at the injection site. Parameter values, as well as modeling choices, are thus assumed equally probable, and +1/−1 design values are end members. The DoE and RS analysis is performed with JMP 8.0 of Statistical Analysis Software, Inc.

Because of its efficiency and flexibility, DoE has been extensively applied to analyzing reservoir static (i.e., pore volume) and dynamic properties (White et al., 2001; Peng and Gupta, 2004). Some studies focus on identifying geologic factors that influence reservoir heterogeneity, and therefore flow behavior (Larue and Friedmann, 2001; Jian et al., 2002; Castellini et al., 2003; Li and White, 2003; Meddaugh et al., 2004; Milliken et al., 2007; Choi et al., 2007). Uncertainty in engineering parameters is ignored, i.e., fixed production scenarios. Others focus on engineering factors only, while fixing the geologic model (Zabalza-Mezghani et al., 2004; Yeten et al., 2005; Li and Friedmann, 2005, 2006; Bourbiaux, 2010). Several studies look at both uncertainty (Wang and White, 2002; Friedmann et al., 2003), while some have incorporated both into reservoir history matching and production optimization (Narahara et al., 2004; Salhi et al., 2005; Zhang et al., 2007; Amudo et al., 2008). In analyzing CO_2 enhanced oil recovery, the DoE and RS analysis has focused on engineering factors, while assuming a fixed geologic model (Wood et al., 2008; Forooghi et al., 2009; Ghomian et al., 2010; O'Dell and Lindsey, 2010; Purwar et al., 2010). In a few cases, permeability variance or anisotropy is varied, although the pattern of reservoir heterogeneity is fixed (Ghomian et al., 2008; Mosse et al., 2010). In studying GCS uncertainty, with a few exceptions (Sifuentes et al., 2009; Liu and Zhang, 2011), most studies adopt the traditional, one-parameter-at-a-time approach (Beni et al., 2011; Liu et al., 2011). To date, few studies investigate the full range of geologic, engineering, and environmental uncertainty sources and their impact on CO_2 predictions. In the following, a study overview is provided, before static and dynamic modeling approaches are described in detail.

3. Method

3.1. Study overview

An uncertainty analysis of CO_2 storage in the Nugget Sandstone is conducted according to DoE and RS principles. Based on subsets of static site data at the Shute Creek gas plant (see section model in Fig. 1), multiple families of geologic models are built at increasing complexity. Using the PB design, important uncertainty factors are identified for each family, before a RS analysis is conducted to assess uncertainty in the predicted CO_2 storage. The study consists of 4 steps:

1. Using subsets of the static site data, generate four families of geologic models with increasing complexity, from a deterministic model with homogeneous porosity (φ) and permeability (k), to a hierarchical stochastic model conditioned to both hard and soft data;
2. For each family, conduct a SA based on the PB design to identify key factors that impact CO_2 storage. These factors are (a) important factors that need to be better characterized, and (b) input to a RS uncertainty analysis;
3. For each family, conduct a RS analysis to assess the CO_2 storage prediction uncertainty. This step consists of: (a) generating a RS design using the important factors identified by the PB design; (b) conducting reservoir simulations according to the RS design and fitting a RS model to the simulation outcome; (c) verifying the RS model at non-RS-design points; (d) creating a prediction envelop of the outcome with the RS model via MC sampling.
4. Over two different time scales, uncertainty outcomes are analyzed and compared among the model families, yielding insights into the effect of model complexity on parameter importance and prediction uncertainty.

To facilitate model comparison, the same amount of CO_2 is injected in all models. The main outcome of interest is the CO_2 mass storage ratio (SR), defined as: SR = (dissolved CO_2 + residual $scCO_2$)/(total injected CO_2), where $scCO_2$ is supercritical-phase CO_2. Residual $scCO_2$ refers to gas trapped in formation pore space due to imbibition, i.e., gas-phase relative permeability hysteresis. (At the depth of the Nugget Sandstone, CO_2 exists in the supercritical phase, before dissolving into the formation brine. To be consistent with terminology of the reservoir simulator, the word "gas" is used here to represent $scCO_2$.) In the deeply buried Nugget Sandstone, in situ groundwater flow is expected to be insignificant, thus dissolved CO_2 is considered trapped. Besides these forms of CO_2, remaining mobile $scCO_2$ (mobile gas) can migrate under viscous and buoyant forces, posing a leakage risk that can be assessed by $(1 - SR)$. The SR is examined over two time scales to evaluate the effect of time on the uncertainty outcomes.

Table 1
Symbols, units, and ranges of the uncertainty factors varied in the DoE. The azimuth is referenced to due east (0 degree). L_1, L_2, and L_3 are modeling choices associated with a categorical factor (see text for detail). CF = common factors; FF = family factors.

Parameter	Symbol	Units	−1	0	+1	Type
Ratio of k_v to k_h	k_v/k_h		0.02	0.2	2.0	CF
Salinity	sal	ppm	10,000	50,000	100,000	CF
Rock compressibility	β	1/[N/m^2]	4.35×10^{-10}	2.03×10^{-9}	3.63×10^{-9}	CF
Temperature at 6500 ft (1981 m) depth	T	Kelvin	310.84	365.01	419.18	CF
Temperature at 12000 ft (3658 m) depth	T	Kelvin	326.14	403.21	480.29	CF
Relative permeability	k_r		L_1	L_2	L_3	CF
Capillary pressure	P_c		L_1	L_2	L_3	CF
Petrofacies modeling method	M_f		L_1	L_2	L_3	FF
Facies Probability	M_p		L_1	L_2	L_3	FF
Multiplier of porosity variogram range	r_φ		0.5	1.0	2.0	FF
Azimuth of porosity variogram	θ_φ	Degree	−5	40	85	FF
Multiplier of petrofacies variogram range	r_f		0.5	1.0	2.0	FF
Azimuth of petrofacies variogram	θ_f	Degree	−5	40	85	FF

3.2. Reservoir static modeling and uncertainty factors

To model CO_2 storage in the Nugget Sandstone, a variety of site characterization data are collected, screened for accuracy, and analyzed. These data include wireline logs, core φ and k, geologic cross sections, isopach maps, and seismic interpretations. As CO_2 storage is known to be affected by residual trapping, relative permeability models were obtained from laboratory experiments on sandstone cores. Capillary pressure, measured on similar cores, was also obtained. Detailed information on data analysis is provided in Li et al. (2011) and is not repeated here. In this study, input parameters for CO_2 simulation are either fixed (those that vary little at a typical storage site) or variable (the so-called "factors"). The latter group is subject to the uncertainty analysis and includes family factors (FF) and engineering/environmental factors or common factors (CF). Table 1 lists the symbols and ranges of these factors.

Family factors are those whose variations control reservoir heterogeneity. For each model family, the choice of the FF depends on its level of complexity (see schematics in Fig. 3). Common factors are shared by all families, and include the ratio of vertical to lateral intrinsic permeability (k_v/k_h), brine salinity (sal), rock compressibility (β), reservoir temperature (T), relative permeability model (k_r), and capillary pressure (P_c). These factors and their uncertainties are considered mostly independent of reservoir heterogeneity and the FF contributing to it, although they exert important controls on CO_2 flow, storage, and partitioning. For example, relative permeability and capillary pressure can significantly affect the amount of residual gas trapped in the pore space. k_v/k_h can influence the lateral extent, size, and shape of the CO_2 plume, which in turn influences residual trapping and CO_2 dissolution. Sal controls the amount of CO_2 dissolution in the formation brine: less dissolution occurs in higher salinities. Rock compressibility influences the evolution of fluid pressure in the reservoir in response to injection: initially higher pressure will propagate to reservoir boundaries, which induces formation brine to flow out of the model, which then modulates reservoir pressure. By affecting phase density, and to a lesser extent, phase viscosity, temperature influences the relative importance of gravity override versus viscous drive from injection. For example, a hotter and more buoyant plume will rise up faster from the injection well toward the reservoir top, which can result in more residual trapping and dissolution per unit time.

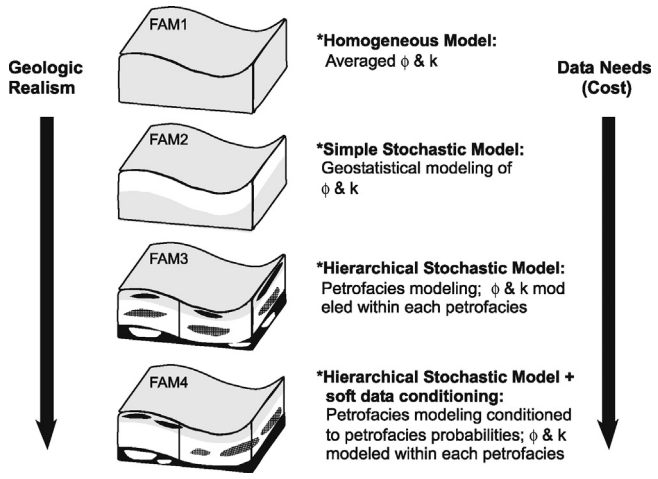

Fig. 3. A schematic diagram of the geologic model families evaluated in this work.

In Table 1, k_r, P_c, petrofacies modeling method, and facies probability are categorical factors: their ranges reflect end-member modeling choices. For example, the −1 end-member of k_r is a relative permeability model of the CO_2 phase that does not exhibit hysteresis, i.e., the imbibition and drainage curves overlap (Fig. 4; top panel). In contrast, the +1 end-member of k_r is a model with significant CO_2 relative permeability hysteresis, i.e., a large residual gas saturation at zero CO_2 relative permeability (Fig. 4; bottom right panel). The −1 model does not contribute to residual trapping as much as the +1 model. The center-point model (marked by 0) is one with a moderate amount of hysteresis, whereby CO_2 residual gas saturation is half that of the +1 model (Fig. 4; bottom left panel). Similarly, the end-member modeling choices for P_c yield results ranging from negligible to significant residual trapping, which influences CO_2 storage. The petrofacies and facies probability modeling is discussed below.

Using subsets of the site data, a suite of increasingly complex geologic model families are built: a homogeneous model (FAM1), a stationary petrophysical model (FAM2), a stationary facies model with sub-facies petrophysical variability (FAM3), and a non-stationary facies model (with sub-facies variability) additionally conditioned to soft data (FAM4) (Fig. 3). These families, representing alternative conceptual models built with increasing site data, share the same external geometry, simulation grid, CO_2 injection design (e.g., well location, injection rate/duration, bottomhole pressure constraint), and boundary conditions (i.e., model is considered part of a larger semi-infinite system, where both the injected CO_2 and formation brine can flow out). The families vary only in how reservoir heterogeneity is represented, as explained below.

For FAM1, FF do not exist, due to the homogeneity assumption—CF are the only ones varied in the SA according to the PB design (Table 2). Average porosity and permeability, calculated from Nugget Sandstone core measurements, are assigned to this model. In contrast, the static model building procedure for FAM2, FAM3, and FAM4 is dictated by the design (Fig. 3): the number of FF increases in response to the increased model complexity. For

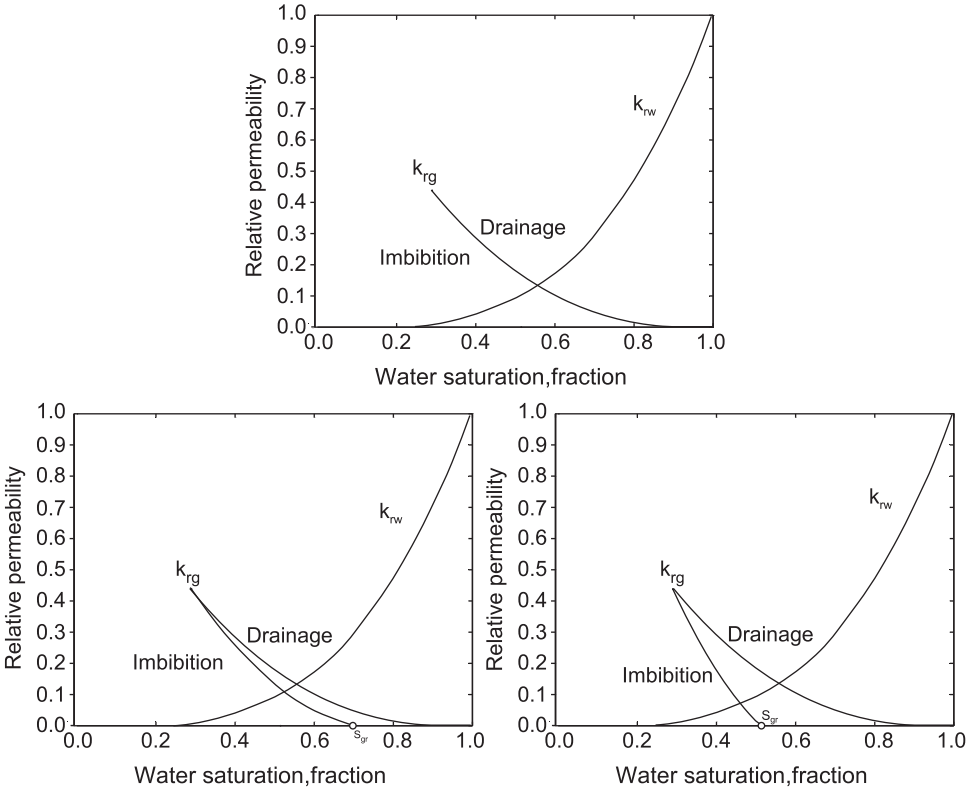

Fig. 4. End member relative permeability models. k_{rw}: relative permeability of brine (not varied in the SA). k_{rg}: relative permeability of $scCO_2$. S_{gr}: residual CO_2 saturation. Top: no hysteresis (−1 end-member); lower left: small hysteresis (center point); lower right, large hysteresis (+1 end-member).

Table 2
PB design for FAM1. Only the common factors are varied. "Run-number" is a simulation ID. For this values and model family, 19 simulations are conducted according to the design. The parameter ranges are listed in Table 1.

Runs	k_v/k_h	sal	β	T	k_r	P_c
Run-1	−1	−1	1	−1	L_2	L_2
Run-2	−1	1	1	1	L_3	L_1
Run-3	1	−1	1	−1	L_2	L_3
Run-4	1	1	1	1	L_3	L_2
Run-5	0	0	0	0	L_1	L_1
Run-6	1	1	1	1	L_3	L_3
Run-7	−1	−1	1	1	L_2	L_1
Run-8	−1	−1	−1	−1	L_3	L_3
Run-9	1	1	1	−1	L_1	L_1
Run-10	1	1	−1	−1	L_2	L_1
Run-11	1	−1	−1	−1	L_3	L_1
Run-12	−1	1	−1	−1	L_1	L_3
Run-13	−1	−1	−1	−1	L_3	L_2
Run-14	−1	1	−1	1	L_2	L_3
Run-15	1	−1	−1	1	L_1	L_2
Run-16	−1	1	1	−1	L_1	L_2
Run-17	1	1	−1	1	L_2	L_2
Run-18	1	−1	1	1	L_1	L_3
Run-19	−1	−1	−1	1	L_1	L_1

Table 3
PB design for FAM2. The parameter values and ranges are listed in Table 1 and Fig. 5.

Runs	r_φ	θ_φ	k_v/k_h	sal	c	T	k_r	P_c
Run-1	−1	1	−1	−1	1	−1	L_1	L_3
Run-2	−1	−1	−1	−1	−1	−1	L_3	L_3
Run-3	−1	−1	1	1	−1	−1	L_2	L_1
Run-4	1	1	1	1	1	1	L_3	L_3
Run-5	1	1	−1	−1	1	1	L_2	L_1
Run-6	−1	1	−1	1	−1	1	L_2	L_3
Run-7	1	1	1	−1	−1	−1	L_1	L_1
Run-8	−1	−1	−1	−1	−1	−1	L_3	L_2
Run-9	1	−1	1	1	−1	1	L_1	L_3
Run-10	−1	1	1	1	1	−1	L_3	L_1
Run-11	1	1	1	1	1	1	L_3	L_2
Run-12	0	0	0	0	0	0	L_1	L_1
Run-13	−1	−1	1	−1	1	1	L_2	L_2
Run-14	−1	−1	−1	1	1	1	L_1	L_1
Run-15	−1	1	1	−1	−1	1	L_1	L_2
Run-16	1	−1	−1	−1	−1	1	L_3	L_1
Run-17	1	−1	1	−1	1	−1	L_2	L_3
Run-18	1	−1	−1	1	1	−1	L_1	L_2
Run-19	1	1	−1	1	−1	−1	L_2	L_2

each family, *a suite of* geologic models exhibiting different φ and k heterogeneity are built, as explained in the following.

FAM2 is a geostatistical petrophysical model with heterogeneous porosity and permeability. Unlike FAM1, where only a single porosity/permeability model is built, a suite of models is built for FAM2, whereby each model exhibits a different heterogeneity pattern. For FAM2, φ is modeled with sequential Gaussian simulation and k is populated from porosity using log-linear transforms. Detail on the variogram analysis, the geostatistical simulation technique, and the development of $\varphi - \log k$ transforms can be found in Li et al. (2011). Compared to FAM1, 2 more uncertainty factors are evaluated by the PB design because of the increased model complexity (Table 3): horizontal φ correlation range and its principal horizontal azimuth (direction of maximum φ correlation). These factors are varied in the SA in addition to the shared CF with FAM1. Uncertainty ranges for these factors are determined by the uncertainty in fitting a horizontal variogram model to the experimental variograms. Due to well sparsity, horizontal variograms are constructed at fewer lag distances, thus horizontal variogram modeling suffers greater uncertainty than vertical variogram modeling. A preliminary horizontal variogram model is fitted to the experimental variograms, with which a best-fit principal maximum φ correlation range is obtained. Given the uncertainty

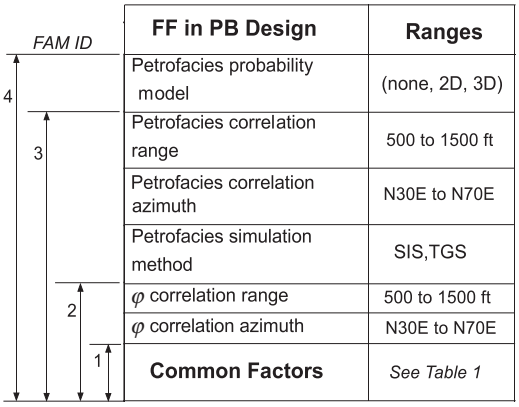

Fig. 5. Family Factors varied in the PB design for each family and their ranges. Numbers denote family ID. SIS: sequential indicator simulation; TGS: truncated Gaussian simulation. Common factors are shared by all model families. Facies and φ correlation range and azimuth are of the horizontal direction. Both two-dimensional (2D) and three-dimensional (3D) facies probability models are created for FAM4.

in the fit, this range is multiplied by a correlation range multiplier, which is varied in the DoE and RS analysis as an uncertain FF.

For FAM3, six (discrete) petrofacies units are first modeled, conditioned to well log data, before the petrophysical properties are modeled within each petrofacies. Information on petrofacies categorization and verification is provided in Li et al. (2011). In addition to the CF and FF of FAM2, 3 family factors reflecting petrofacies modeling uncertainty are added (Fig. 5): petrofacies correlation range, azimuth, and modeling method. Similar to porosity modeling, horizontal facies variogram modeling suffers greater uncertainty than vertical facies variogram modeling, thus both petrofacies correlation range and azimuth are of the horizontal direction. A preliminary horizontal variogram model is fitted to the experimental variogram, with which a best-fit principal maximum petrofacies correlation range is obtained. It is multiplied by a correlation range multiplier which is varied in the DoE and RS analysis as an uncertain FF. Two facies modeling methods are also tested: Sequential indicator simulation (SIS) versus truncated Gaussian simulation (TGS) (Schlumberger, 2009b). The decision to adopt these techniques is to (a) be consistent with previous modeling studies (see Li et al. (2011) and references therein), and (b) explore the influence of alternative modeling techniques on creating reservoir heterogeneity. Given the limited well data at the injection site, either technique may be appropriate, as there is no evidence suggesting that SIS is more suitable than TGS. Compared to FAM2, a greater model complexity is explored (Table 4): more combinations of reservoir variability are evaluated, including the *simultaneous* variation of petrofacies and sub-petrofacies porosity and permeability.

In FAM4, in addition to the CF and FF of FAM3, petrofacies modeling is constrained by a facies probability model (soft data), introducing one more FF into the list of uncertainty factors: no conditioning versus conditioning to a 2D facies probability map versus conditioning to a 3D facies probability cube. Petrofacies modeled with SIS or TGS, when conditioned to facies probability, becomes non-stationary. The 2D probability map is created from interpolating vertically integrated petrofacies types at wells, which contains a trend to preserve geological realism, i.e., one or

Table 4
PB design for FAM3. The parameter values and ranges are listed in Table 1 and Fig. 5.

Runs	r_f	θ_f	r_φ	θ_φ	k_v/k_h	sal	c	T	k_r	P_c	M_f
Run−1	1	1	−1	1	1	−1	1	−1	L_1	L_2	L_1
Run-2	1	1	1	−1	1	1	−1	1	L_2	L_3	L_1
Run-3	1	1	1	−1	1	1	−1	1	L_3	L_1	L_1
Run-4	−1	−1	−1	−1	−1	−1	−1	−1	L_3	L_3	L_1
Run-5	−1	−1	−1	1	1	1	−1	1	L_3	L_2	L_2
Run-6	−1	−1	1	1	1	−1	1	1	L_3	L_2	L_1
Run-7	−1	−1	1	1	1	−1	1	1	L_1	L_3	L_1
Run-8	1	−1	−1	−1	1	1	1	−1	L_3	L_2	L_2
Run-9	1	1	−1	1	1	−1	1	−1	L_2	L_3	L_1
Run-10	0	0	0	0	0	0	0	0	L_1	L_1	L_1
Run-11	1	−1	−1	−1	1	1	1	−1	L_1	L_3	L_2
Run-12	−1	1	1	−1	1	−1	−1	−1	L_2	L_2	L_2
Run-13	−1	1	1	1	−1	1	1	−1	L_2	L_3	L_2
Run-14	1	−1	1	1	−1	1	−1	−1	L_3	L_1	L_1
Run-15	−1	−1	−1	−1	−1	−1	−1	−1	L_2	L_2	L_1
Run-16	1	−1	1	1	−1	1	−1	−1	L_2	L_3	L_1
Run-17	1	−1	1	−1	−1	−1	1	1	L_2	L_2	L_2
Run-18	−1	1	−1	−1	−1	1	1	1	L_2	L_1	L_1
Run-19	−1	−1	−1	1	1	1	−1	1	L_2	L_1	L_2
Run-20	−1	−1	1	1	1	−1	1	1	L_2	L_1	L_1
Run-21	1	1	−1	1	−1	−1	−1	1	L_1	L_1	L_2
Run-22	−1	1	−1	−1	−1	1	1	1	L_3	L_2	L_1
Run-23	1	−1	1	1	−1	1	−1	−1	L_1	L_2	L_1
Run-24	−1	1	1	−1	1	−1	−1	−1	L_3	L_3	L_2
Run-25	1	−1	−1	−1	1	1	1	−1	L_2	L_1	L_2
Run-26	1	1	−1	1	−1	−1	−1	1	L_3	L_3	L_2
Run-27	1	−1	1	−1	−1	−1	1	1	L_1	L_1	L_2
Run-28	−1	−1	−1	1	1	1	−1	1	L_1	L_3	L_2
Run-29	1	1	−1	1	−1	−1	−1	1	L_2	L_2	L_2
Run-30	−1	1	1	1	−1	1	1	−1	L_3	L_1	L_2
Run-31	−1	1	1	−1	1	−1	−1	−1	L_1	L_1	L_2
Run-32	1	1	−1	1	1	−1	1	−1	L_3	L_1	L_1
Run-33	1	1	1	−1	−1	1	−1	1	L_1	L_2	L_1
Run-34	1	−1	1	−1	−1	−1	1	1	L_3	L_3	L_2
Run-35	−1	1	1	1	−1	1	1	−1	L_1	L_2	L_2
Run-36	−1	1	−1	−1	−1	1	1	1	L_1	L_3	L_1
Run-37	−1	−1	−1	−1	−1	−1	−1	−1	L_1	L_1	L_1

Table 5
PB design for FAM4. The parameter values and ranges are listed in Table 1 and Fig. 5.

Runs	r_f	θ_f	r_φ	θ_φ	k_v/k_h	sal	c	T	k_r	P_c	M_f	M_p
Run-1	−1	1	−1	−1	−1	−1	1	1	L_2	L_1	L_1	L_2
Run-2	−1	1	−1	−1	−1	−1	1	1	L_3	L_2	L_1	L_3
Run-3	1	1	−1	1	1	1	−1	1	L_1	L_2	L_1	L_3
Run-4	1	1	−1	1	−1	−1	−1	1	L_3	L_3	L_2	L_1
Run-5	−1	−1	−1	−1	−1	−1	−1	−1	L_1	L_1	L_1	L_1
Run-6	1	−1	−1	−1	1	1	1	−1	L_2	L_1	L_2	L_1
Run-7	−1	−1	1	1	1	1	1	1	L_1	L_3	L_1	L_2
Run-8	0	0	0	0	0	0	0	0	L_1	L_1	L_1	L_1
Run-9	1	1	−1	1	−1	−1	−1	1	L_2	L_2	L_2	L_2
Run-10	−1	1	1	1	−1	−1	1	−1	L_2	L_3	L_2	L_3
Run-11	1	1	1	−1	1	1	−1	1	L_2	L_3	L_1	L_2
Run-12	1	−1	1	1	−1	−1	−1	−1	L_2	L_3	L_1	L_1
Run-13	1	−1	1	1	−1	−1	−1	−1	L_1	L_2	L_1	L_3
Run-14	1	1	1	−1	1	1	−1	1	L_1	L_2	L_1	L_1
Run-15	1	1	−1	1	1	1	1	−1	L_3	L_1	L_1	L_2
Run-16	−1	−1	1	1	1	1	1	1	L_2	L_1	L_1	L_3
Run-17	−1	1	−1	−1	−1	−1	1	1	L_1	L_3	L_1	L_1
Run-18	−1	−1	−1	1	1	1	−1	1	L_1	L_3	L_2	L_2
Run-19	1	−1	1	−1	−1	−1	1	1	L_2	L_2	L_2	L_2
Run-20	−1	−1	−1	−1	−1	−1	−1	−1	L_2	L_2	L_1	L_2
Run-21	1	1	−1	1	−1	−1	−1	1	L_1	L_1	L_2	L_2
Run-22	−1	−1	−1	−1	−1	−1	−1	−1	L_3	L_3	L_1	L_3
Run-23	−1	−1	−1	1	1	1	−1	1	L_3	L_2	L_2	L_1
Run-24	−1	−1	−1	−1	1	1	1	−1	L_3	L_2	L_2	L_2
Run-25	1	1	−1	1	1	1	1	−1	L_2	L_3	L_1	L_1
Run-26	−1	−1	−1	1	1	1	−1	1	L_2	L_1	L_2	L_3
Run-27	−1	1	1	1	−1	−1	1	−1	L_1	L_2	L_2	L_2
Run-28	−1	1	1	1	−1	−1	1	−1	L_3	L_1	L_2	L_1
Run-29	1	1	1	−1	1	1	−1	−1	L_3	L_3	L_2	L_2
Run-30	1	−1	1	−1	−1	−1	1	1	L_3	L_3	L_2	L_3
Run-31	1	−1	−1	−1	1	1	1	−1	L_1	L_3	L_2	L_3
Run-32	1	1	1	−1	1	1	−1	1	L_3	L_1	L_1	L_3
Run-33	−1	1	1	−1	1	1	−1	−1	L_1	L_1	L_2	L_3
Run-34	−1	1	1	−1	1	1	−1	−1	L_2	L_2	L_2	L_1
Run-35	1	−1	1	1	−1	−1	−1	−1	L_3	L_1	L_1	L_2
Run-36	1	−1	1	−1	−1	−1	1	1	L_1	L_1	L_2	L_1
Run-37	−1	−1	1	1	−1	−1	1	1	L_3	L_2	L_1	L_1

more petrofacies may disappear or become replaced by another petrofacies. For each of the 6 petrofacies units (previously modeled in FAM3 as a stationary geostatistical population conditioned only to well petrofacies or the "hard data"), petrofacies modeling is additionally constrained by the probability map. The 3D probability cube, created from the same well data, additionally accounts for petrofacies non-stationarity with depth. How the probability models are created and used to condition petrofacies modeling is described elsewhere (Ma et al., 2009), and is not repeated here. The PB design for FAM4 is shown in Table 5.

Based on the PB design, families of geostatistical reservoir models are created. For each family, a porosity realization is shown (Fig. 6), corresponding to the center runs of the design (all parameters assume median values). Depending on the modeling method and the amount of supporting data, different heterogeneities are created. As expected, porosity model of FAM2 has less internal structure than those of FAM3 and FAM4. By conditioning to facies probabilities, FAM4 honors the non-stationary facies trends inferred from well data. The comparison here illustrates the difference in mean heterogeneity representation among the families. Additional variability exists among the models of each family, where parameters (and modeling method) are varied according to the experimental design.

3.3. Dynamic modeling of CO_2 injection and monitoring

For all families, the same CO_2 injection test is simulated using GASWAT of Eclipse 300, a multiphase compositional simulator that models gas/aqueous phase equilibrium through an equation of state (EOS) (Schlumberger, 2009a). Two phases are considered: a CO_2-rich supercritical phase and a H_2O-rich liquid phase. CO_2 density is computed using a cubic EOS tuned to experimental measurements. Liquid density is corrected for total dissolved solids. Between the two phases, three components (CO_2, H_2O, NaCl) are modeled. CO_2 and H_2O can exist in both phases, but NaCl can only exist in the liquid phase. GASWAT solves the pressure and molar density of each component. Mole fractions of the components in the phases are then computed through a flash process, in which mutual solubilities of CO_2 and H_2O are calculated to match experimental data. Initial reservoir fluid pressure is hydrostatic, with a reference pressure of 6372.85 psi (~44 MPa) at a true vertical depth of 14,000 ft (4267 m) (a brine density of 1.05 g/cm^3 is assumed). With GASWAT, temperature of the reservoir can vary with depth, which determines the initial fluid properties (no energy balance equation is solved). A temperature field is assigned to the model by interpolating and extrapolating data from temperature logs (Li et al., 2011).

Model boundaries are represented by a Fetkovich analytical aquifer of a large radius and thickness (Schlumberger, 2009a), which ensures an open boundary that allows the formation brine, and later scCO_2, to flow out. This is consistent with a reservoir model in communication with a larger aquifer (see the regional model in Fig. 1). The injection well is located at the Shute Creek gas plant and is fully perforated in the sandstone. To prevent fluid overpressure, an injector bottomhole pressure (BHP) constraint is set at 1.8 times the hydrostatic pressure (Li et al., 2011). The constraint is used to monitor the actual calculated BHP at the injector well screen which fluctuates with time for a fixed mass injection rate. If this rate is too high, the actual injector BHP can rise above this constraint, at which time Eclipse 300 will adjust the rate

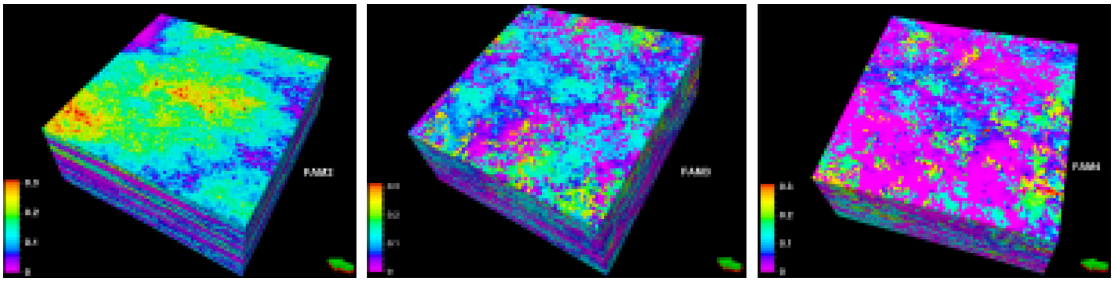

Fig. 6. A porosity model realization for FAM2, FAM3, and FAM4, corresponding to the center run of the respective PB design.

down, which makes it difficult to ensure that all the simulation runs inject the same amount of CO_2. Due to adverse parameter combinations, some model runs may have low injectivity, i.e., low reservoir permeability. The injection rate must be chosen to ensure that all simulations proceed normally without the injector being shut-in due to high BHP. After trial and error with different rates, CO_2 is injected for 50 years at a fixed rate of 1/10 Mt/year (1.0×108 kg/year), selected so that, for the given injector BHP constraint, all model families can accommodate the same amount of the injected CO_2. To model industrial scale injection at a rate of 10 to 50 Mt/year, however, more than one injectors, and possibly brine producers, are needed (Stauffer et al., 2009a). These scenarios are not investigated. Because of the low injection rate and the specified boundary conditions, formation brine is continuously displaced out of the model by the pressure increase at the injector. Reservoir fluid pressure never rises high enough to fracture the formation and is therefore not examined as an outcome.

Parameters important to predicting the CO_2 storage ratio is first identified for each model family at the end of injection, along with the uncertainty in the storage ratio. Because model complexity on the long-term fate of CO_2 is also of interest, a post-injection monitoring phase is simulated. For all models, the total simulation time is 3000 years. This timeframe is selected because gravity migration of $scCO_2$ occurs continuously, long after the injection has ceased. Over the monitoring period, effect of large-scale reservoir heterogeneity on migration and trapping can come into play. In GCS modeling, both shorter and longer time scales have been examined. In general, shorter monitoring times were simulated to evaluate the effect of multiphase flow on CO_2 capillary trapping and fluid pressure responses, while longer monitoring times were simulated to understand the long-term fate of CO_2 after a significant period of dissolution and fluid–rock interaction. Here, an intermediate time scale (3000) was chosen, so that both the short-term and long-term outcomes related to CO_2 storage and migration can be evaluated, e.g., CO_2 storage ratio at the end of injection and monitoring, gas plume shape, gas footprint, etc. The simulation time does not extend much longer than 3000 years, because by that time $scCO_2$ in many runs will dissolve out and there would not be a gas plume left for assessing the footprint.

Finally, given the number of DoE runs that are simulated, computational effort of this study is significant: for the combined DoE and RS analysis, 404 reservoir simulation runs were performed. Each run has taken from overnight to up to 2 weeks to complete. All simulations are checked for accuracy and proper convergence, before the results are analyzed. For all families, the amount of the injected gas is examined to ensure that all families inject the same amount of CO_2.

4. Results

Results of this uncertainty study are presented in 4 sections: (1) screening test outcomes; (2) RS modeling and verification; (3) MC analysis to assess the storage ratio uncertainty; (4) visualization of end-member CO_2 plumes and footprints. In each section, results are analyzed at two output times: end of injection (EOI) and end of monitoring (EOM).

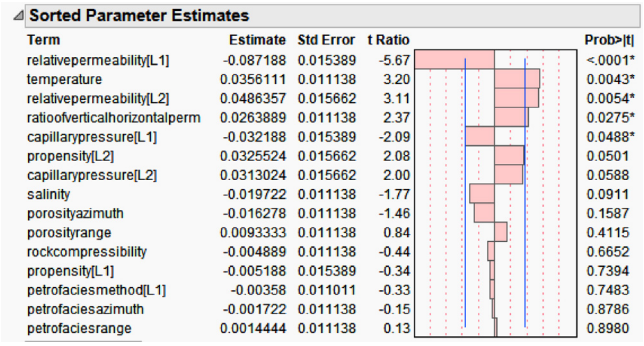

Sorted Parameter Estimates

Term	Estimate	Std Error	t Ratio	Prob>|t|
relativepermeability[L1]	-0.087188	0.015389	-5.67	<.0001*
temperature	0.0356111	0.011138	3.20	0.0043*
relativepermeability[L2]	0.0486357	0.015662	3.11	0.0054*
ratiooverticalhorizontalperm	0.0263889	0.011138	2.37	0.0275*
capillarypressure[L1]	-0.032188	0.015389	-2.09	0.0488*
propensity[L2]	0.0325524	0.015662	2.08	0.0501
capillarypressure[L2]	0.0313024	0.015662	2.00	0.0588
salinity	-0.019722	0.011138	-1.77	0.0911
porosityazimuth	-0.016278	0.011138	-1.46	0.1587
porosityrange	0.0093333	0.011138	0.84	0.4115
rockcompressibility	-0.004889	0.011138	-0.44	0.6652
propensity[L1]	-0.005188	0.015389	-0.34	0.7394
petrofaciesmethod[L1]	-0.00358	0.011011	-0.33	0.7483
petrofaciesazimuth	-0.001722	0.011138	-0.15	0.8786
petrofaciesrange	0.0014444	0.011138	0.13	0.8980

Fig. 7. Screening test result for FAM4 at the end of injection at the 95% significance level. Statistically significant factors include relative permeability, temperature, capillary pressure, and k_v/k_h. "Propensity" refers to facies conditioning by the facies probability models.

4.1. Screening tests

Screening test results of all model families are examined with MANOVA to determine the key uncertainty factors that influence the predicted CO_2 storage ratio at a significance level of 95%. As a key statistics of MANOVA, *t*-ratio is used to determine the effect of each uncertainty factor on CO_2 storage. For FAM4, at the end of injection, the uncertainty factors are ranked (Fig. 7). At both time scales, the important factors (ranked from the most important to least important) are also listed in Table 6. Out of the 12 factors screened by the PB design (Table 5), 3 factors (petrofacies modeling method, petrofacies variogram range, petrofacies variogram azimuth) are identified as insignificant at *both* time scales, while 9 factors are identified as significant at one or both time scales. These 9 factors are used in the subsequent RS design, which involves additional simulations. This approach of coupling the screening design with the RS design is implemented for each model family.

Table 6
Significant factors that impact the predicted CO_2 storage ratio at the 95% significance level. For each model family, at both time scales (EOI and EOM), the significant factors are identified using *t*-ratio. The factors are ranked from the most important to the least important on influencing the storage ratio.

Family	Significant factors (end of injection)	Significant factors (end of monitoring)
FAM1	k_r, P_c, k_v/k_h, T	sal, T, k_r, k_v/k_h
FAM2	k_r, P_c, T, sal	k_r, T, β, P_c
FAM3	k_r, k_v/k_h, T, β	k_r, sal, porosity correlation range, P_c
FAM4	k_r, T, k_v/k_h, P_c	k_r, T, facies soft data conditioning, sal

For all families, key uncertainty factors influencing the storage ratio are summarized in Table 6. For each family, the important factors are observed to change with time, reflecting the different flow physics that dominates CO_2 flow, before and after injection. When comparing the important factors across the families (at the same time), when complexity in representing reservoir heterogeneity is not modeled, the important uncertainty parameters are dominated by the engineering/environmental factors. When complexity is increased, geologic uncertainty factors become more important, but only over the monitoring time. Clearly, these factors, which influence permeability heterogeneity, become more important as CO_2 flows away from the injector and continuously experiences large-scale heterogeneities during its post-injection migration.

4.2. RS modeling and verification

For each family, at each time scale, the PB design has identified a number of important uncertainty factors, with which a RS design is generated to create a proxy model for reservoir simulation. The RS designs are typically of higher resolution than the screening design, thus additional simulations are needed. The number of RS runs is 49 (FAM1), 49 (FAM2), 97 (FAM3), 97 (FAM4) (detailed designs are not shown). A second order polynomial is adopted as the RS model, which is fitted to the simulation outcomes. For each family, two storage ratio RS models are created, one for each time scale. These models are verified by comparing their predictions to the simulated storage ratios that were not used in generating the RS models, i.e., at the PB design points. Though such verification can overestimate the RS error, this comparison still yields relatively small errors. Table 7 presents a summary statistics of the RS model errors: error means are close to 0.0, standard deviations are generally small and, with minor exceptions, error distributions are symmetrical around the means (Fig. 8). When comparing the errors across the families (at the same time), interestingly, error appears to grow with increasing model complexity. This is attributed to the fact that, as model complexity increases, more factors come into play (Fig. 5), resulting in more uncertainty sources contributing to the RS errors. Moreover, had the verification points been selected internal to the parameter space boundaries, the RS error is expected to be smaller. Given these results, the RS models are considered adequate proxy models for reservoir simulation and are used in the subsequent MC analysis.

4.3. MC analysis

For each family, at each time scale, the response surface model is used to assess the prediction uncertainty of the storage ratio (SR), which arises from the uncertain input factors including family factors and common factors. This analysis is conducted by running 100,000 MC simulations with the RS model, randomly sampling the important factors (i.e., axes of the RS model) according to their respective *pdfs*. A drawing of a random vector of the input factors gives rise to one RS-predicted storage ratio. After 100,000 drawings, an experimental cumulative distribution function (*cdf*) of the SR, or the *exhaustive cdf*, is created (Fig. 9 for FAM4; solid line). As expected, the range of the SR is centered at a higher value at the end of monitoring than that at the end of injection. A set of MC runs usually takes less than one second to complete on a PC workstation. It must be cautioned, however, that because the RS models contain errors, they are imperfect representations of the true (unknown) prediction space. For a given system, these errors may be higher or lower depending on the RS design and the fitted model. In general, the RS error decreases with increasing resolution of the design, but more full-physics simulations are needed. The MC-predicted storage ratio ranges and *cdfs* are therefore approximations.

From the same RS design runs, a non-exhaustive *cdf* of the SR is also constructed for both time scales (Fig. 9 for FAM4; dashed line). For all families, at both time scales, these two sets of *cdfs* are comparable, although the *cdfs* based on the RS design runs are less smooth and tend to underestimate the extremes in the storage ratio, as shown by the exhaustive *cdf*. For example, for FAM4, the *minimum* storage ratio predicted by the MC runs is 5% (EOI) and 18% (EOM), respectively. In comparison, the minimum storage ratio from the RS design runs is much higher at 16% (EOI) and 30% (EOM), doubling or tripling the MC projections. This illustrates the importance of exploring the full parameter space in a prediction uncertainty analysis, which is facilitated by the RS models.

After MC samplings, *cdfs* of the RS-predicted storage ratios are compared among the families, at both time scales (Fig. 10). Results suggest a large SR uncertainty, given the uncertainties in model parameters and modeling choices: at the end of injection, SR predicted by all families varies from 5% to 60%; at the end of monitoring, it varies from 18% to 100%. For *each* family, the large variability in the SR is largely controlled by parameter uncertainty (FAM1), or both parameter and within-family conceptual model uncertainties (see Section 4.1 for the important factors identified for each family). The SR uncertainty, however, does not differ significantly among the different *modeling choices* that created these families. For example, at the end of injection, mean SR predicted by different families varies only from 26–33%; at the end of monitoring, its varies from 73–82%. At a given time, variability in the mean SR that is due to different modeling choices is only about 7–9%. Clearly, for the Nugget Sandstone, different modeling choices do not lead to significant differences in the predicted range of the SR, although the shapes of the *cdfs* differ among the families, suggesting different modalities. The SR distribution of FAM4 is more Gaussian (unimodality), which may reflect its greater number of random input factors.

4.4. Plume predictions

For each simulation, three-dimensional CO_2 plumes can be visualized at any time by plotting both $scCO_2$ saturation (i.e., mobile + trapped gas) and dissolved CO_2 mole fraction in brine. The approximate end-member plumes are shown for each family, which are predicted by the RS design runs with the minimum (Fig. 11) and maximum storage ratios (Fig. 12) *at the end of monitoring*, i.e., long-term storage is of interest. The $scCO_2$ plumes corresponding to the lowest (Fig. 11) and highest storage ratios (Fig. 12) are also visualized at the end of injection (left columns in both figures). In general, factors that contribute to a high storage ratio tend to create a larger $scCO_2$ plume before it is dissolved out. During gas migration, more residual gas trapping is expected when the plume size is large. A larger plume also experiences greater dissolution, as more $scCO_2$ is in contact with fresh brine per unit time.

All model families predicting minimum SRs at the end of monitoring have also developed gravity-stable flow (Fig. 11), whereas the injected $scCO_2$ has a higher density than formation brine and gas migration is toward the bottom of the reservoir. By inspecting the input factors, these runs are characterized with cooler formation temperatures, higher (injection) fluid pressures, and higher brine salinities. Cooler temperature and higher pressure give rise to a dense and more compact plume that does not spread out much.

Table 7
Summary statistics of the RS model error for each family at both time scales. RS model error = RS-predicted storage ratio – simulated storage ratio at the PB design points.

Family	EOI [min, mean, max, std]	EOM [min, mean, max, std]
FAM1	[−0.064, 0.000, 0.042, 0.006]	[−0.060, 0.004, 0.061, 0.008]
FAM2	[−0.030, 0.018, 0.066, 0.007]	[−0.110, 0.041, 0.130, 0.012]
FAM3	[−0.078, −0.002, 0.077, 0.005]	[−0.130, 0.014, 0.190, 0.013]
FAM4	[−0.350, −0.040, 0.210, 0.017]	[−0.290, −0.009, 0.360, 0.020]

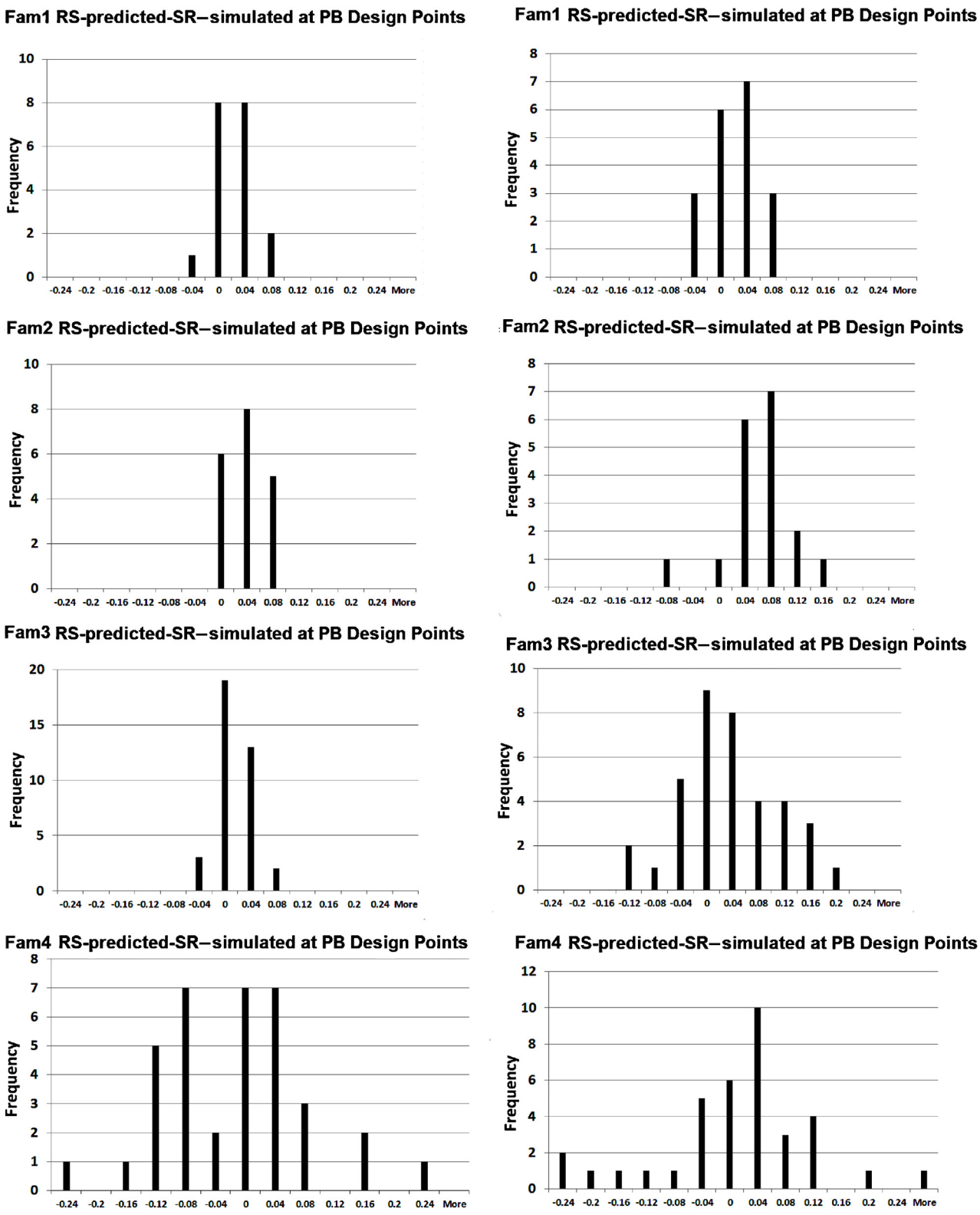

Fig. 8. Histogram of the RS model error at (left) the end of injection and (right) the end of monitoring.

Higher salinities result in less dissolution. Both lead to a lower SR. However, despite the low SR, these runs yield a high storage security because of gravity-stable migration and the fact that $scCO_2$ at the bottom of the reservoir will eventually dissolve out. Moreover, all families predicting maximum SRs at the end of monitoring have developed buoyancy-driven upward migration (Fig. 12). In these cases, warmer formation temperatures, lower pressures, and lower salinities dominate the plume behavior: warmer temperature gives rise to a larger and more buoyant plume, which contributes to more residual trapping and dissolution. In the meantime, higher density contrast between $scCO_2$ and brine results in a greater distance traveled by the mobile gas per unit time, which can be visualized

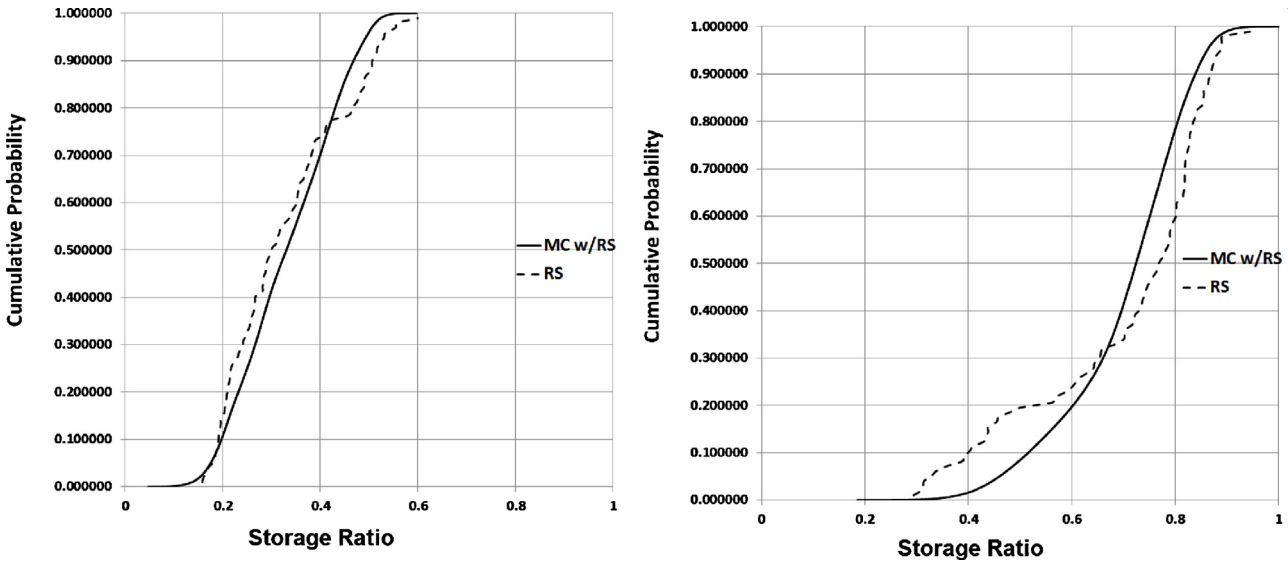

Fig. 9. Cumulative distribution function (*cdf*) of the storage ratio for FAM4: (left) end of injection; (right) end of monitoring. "MC w/RS" is generated with 100,000 MC simulations (exhaustive *cdf*); "RS" is the *cdf* constructed using results of the 97 response surface design runs.

by examining the dissolved CO_2 plume at the end of monitoring (third column of this figure). For each family, size of the dissolved gas plume indicates the maximum extent of the mobile gas plume (and therefore the trapped gas) before it is dissolved out. Compared to the dissolved gas plumes of Fig. 11 (which similarly indicate the maximum extent of the gas plumes), these plumes are more extensive in size. Because the non-exhaustive *cdfs* from the RS design runs can underestimate the exhaustive *cdfs* (Fig. 9), for each family, the dissolved plume corresponding to the true maximum SR could be even more extensive (or, the dissolved plume corresponding to the true minimum SR could be more compact).

Comparing plume predictions across the families, FAM1 predicts the classic plume shapes (either the $scCO_2$ plume or the dissolved plume), which are slightly asymmetrical due to the small formation tilt. The shapes become more irregular as more heterogeneity and model complexity is built into the families. In the lowest-storage-ratio scenarios (Fig. 11), CO_2 footprint, defined as the size of the $scCO_2$ plume at the reservoir top, is negligible at both time scales, because the plumes have sunk to the formation bottom. In comparison, the footprint is more significant in the highest-storage-ratio scenarios (Fig. 12). Moreover, most of the CO_2 is dissolved out by the end of monitoring. Because of the open boundary conditions assigned to the simulations, some mobile gas will migrate out of the bottom (lowest-SR) or top (highest-SR) reservoir boundaries. At the proposed injection site, for the engineering and geologic uncertainty factors identified, long-term leakage risk is considered small. This is because, in the lowest-storage-ratio cases, gravity-stable gas plume is predicted by all model families. In the highest-storage-ratio cases, gas plume footprints at the end of monitoring is negligible because of significant dissolution (although a small fraction of the mobile $scCO_2$ has leaked out of the reservoir top). True behavior of the CO_2 plume likely lies between these extremes, which together suggests good storage capacity and low leakage risk. In the lowest-SR cases, given sufficient time, $scCO_2$ will eventually dissolve out while being gravity-stable; in the highest-SR cases, $scCO_2$ will have diminishing footprints over time.

5. Discussion

For the simulation runs exhibiting gravity-stable flow, mixture densities predicted by the EOS of GASWAT are inspected. Under certain conditions (e.g., low formation temperature as controlled

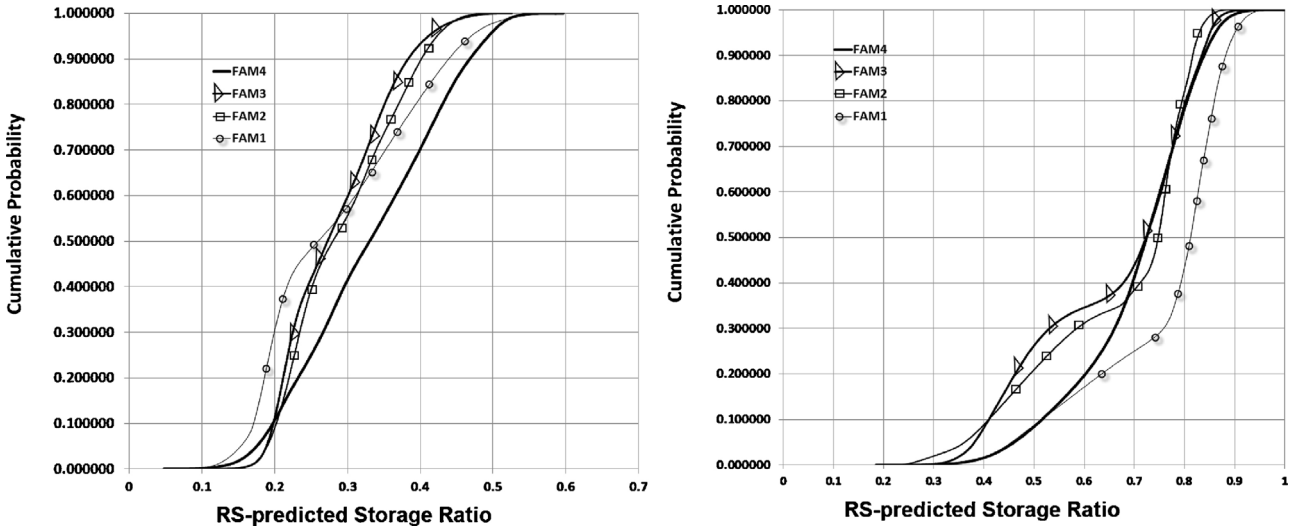

Fig. 10. Cumulative distribution function of the storage ratio predicted by the MC runs for all families: (left) end of injection; (right) end of monitoring.

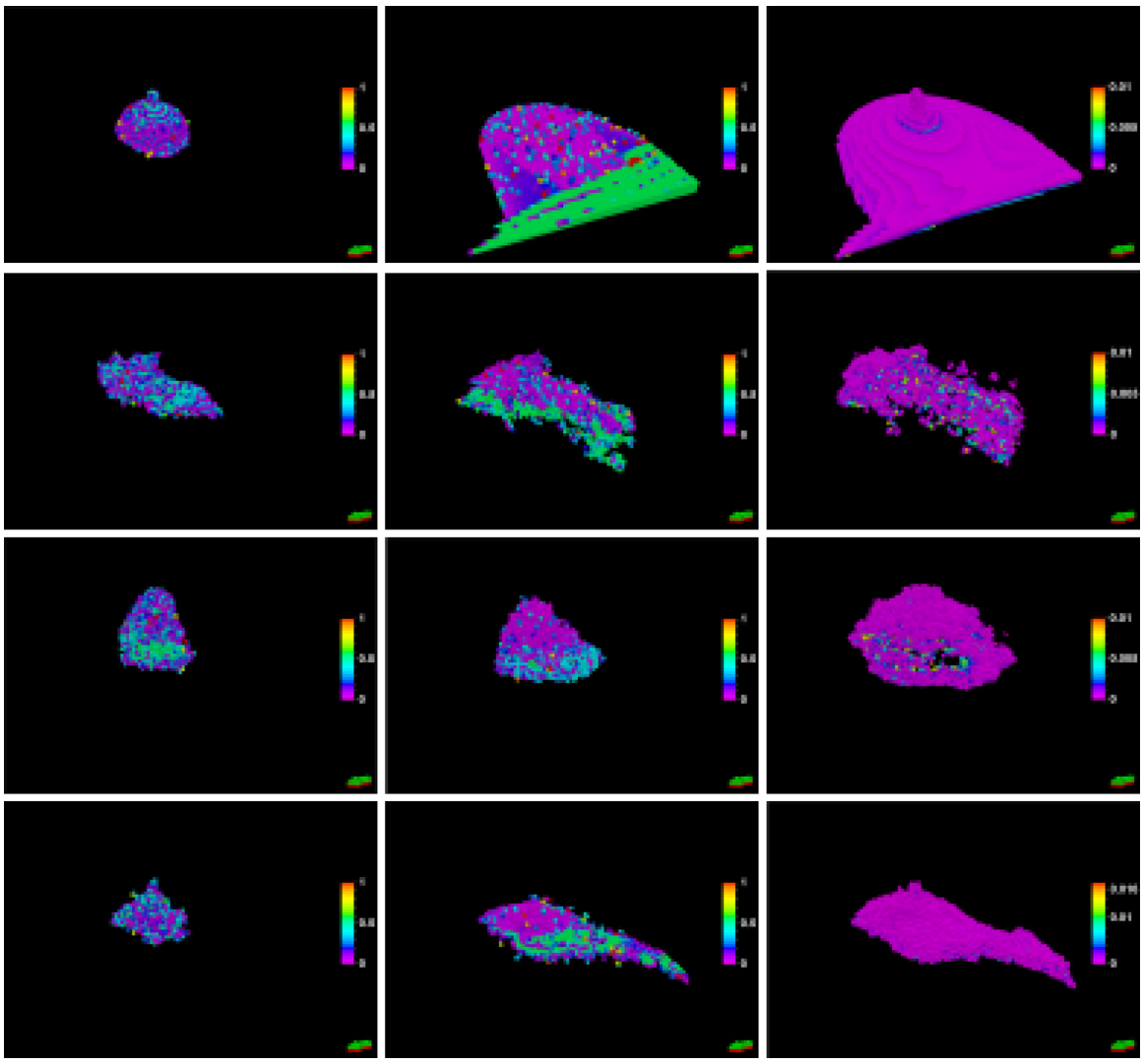

Fig. 11. The lowest-storage-ratio scenario (i.e., minimum CO_2 SR at the end of monitoring) as predicted by the RS design runs for each family (FAM1: first row; FAM2: second row; FAM3: third row; FAM4: fourth row). (Left column) total gas (mobile + trapped CO_2) saturation at the end of injection; (middle column) total gas saturation at the end of monitoring; (right column) dissolved CO_2 (mole fraction) in brine at the end of monitoring. Arrow points North.

by a small geothermal gradient, combined with high formation fluid pressure due to low injectivities), the scCO_2-rich phase (with a small amount of H_2O dissolved in it) can have higher mixture densities than the H_2O-rich phase (with a small amount of CO_2 in it). In Lu et al. (2009), under certain temperature and pressure conditions, when a certain EOS is implemented, CO_2 dissolution in brine can cause brine to become less dense than pristine brine. Firoozabadi and Cheng (2010) pointed out that under sufficiently high pressure, "CO_2 density can be higher than water density", and "There is much theoretical work in the literature on buoyancy-driven flow in CO_2-liquid systems. A restrictive assumption in most cases is the fixed interface between the CO_2-rich and water-rich phases. Because of the large swelling of the water, a fixed boundary may not be a good assumption." The EOS describing mixture densities are being actively researched. If the GASWAT EOS for predicting mixture densities is adequate for the range of temperature and pressure conditions that are encountered in the DoE simulations, this study has shown that gravity-stable migration is possible under suitable conditions. However, to better understand deep injection, more research into mixture EOS needs to be carried out.

In this work, though stochastic techniques are used to generate heterogeneity to populate the model families, realization-based uncertainty analysis is not conducted, which leads to significant computational savings, as hundreds to thousands of heterogeneity realizations can be populated with a single geostatistical modeling technique, and given a single set of the spatial parameters. Potential variability in the RS outcomes due to stochastic fluctuations from multiple realizations is generally considered smaller than that due to uncertainty in facies and petrophysical property variations (Li et al., 2011). Though the DoE methodology is employed here, other uncertainty techniques including those that create proxy models exist (Razavi et al., 2012). For example, with Markov Chain MC techniques, both parameters and conceptual models were evaluated for their impact on modeling radionuclide transport (Ye et al., 2009). These surrogate techniques can be adapted to analyze CO_2 problems and their accuracy and efficiency compared to the DoE methodology. After dynamic data are collected from an actual injection test, RS-based history matching can be carried out for all families to further constrain their parameters. Because these families are largely consistent with the same site data, calibration-enabled uncertainty analysis can be used to assess model likelihoods, with which a subset of the most likely models may be selected to further reduce the uncertainty in prediction (Ye et al., 2010).

This study explores the effect of different conceptual modeling assumptions on parameter importance and prediction uncertainty.

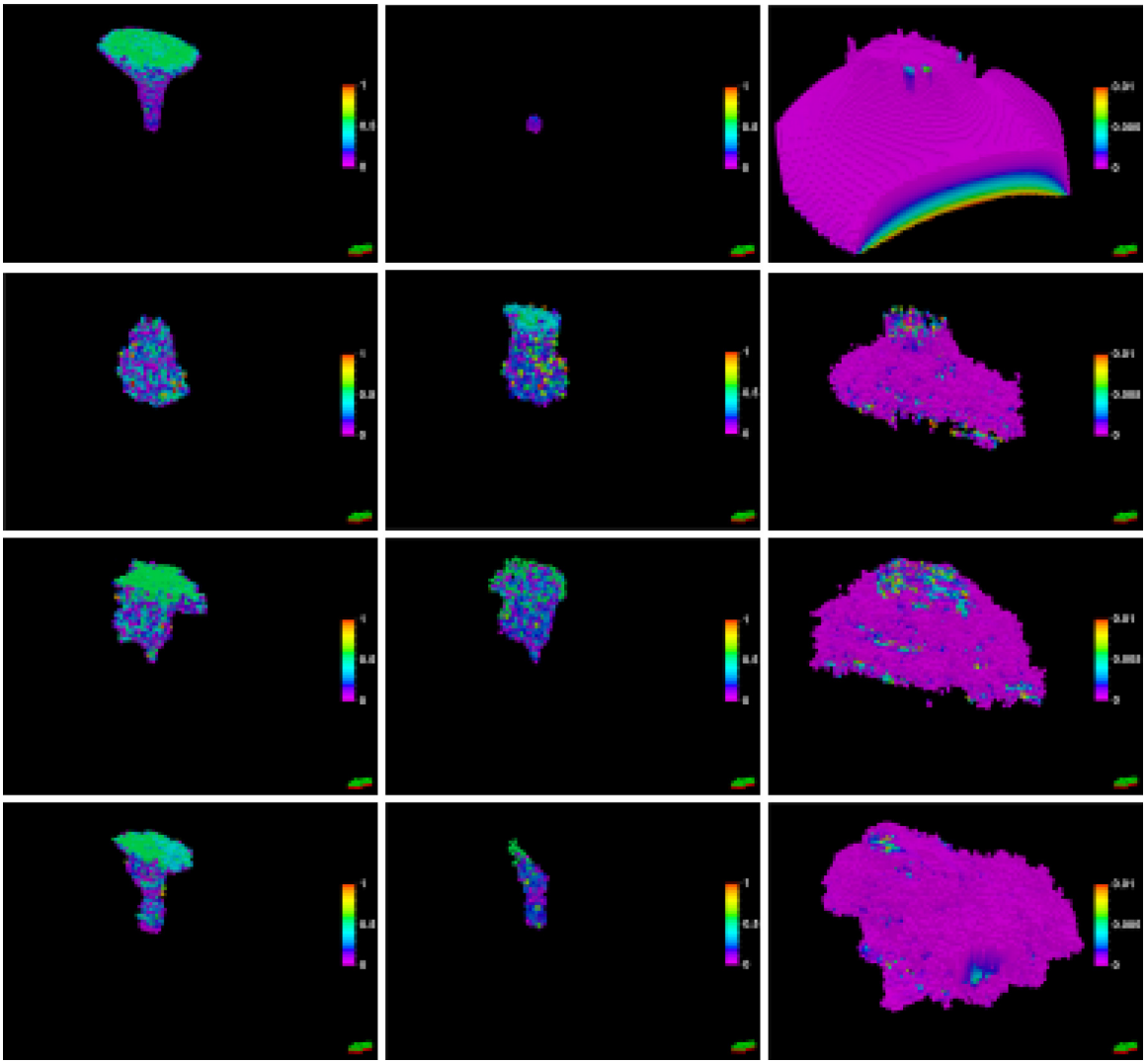

Fig. 12. The highest-storage-ratio scenario (i.e., maximum CO_2 SR at the end of monitoring) as predicted by the RS design runs for each family (FAM1: first row; FAM2: second row; FAM3: third row; FAM4: fourth row). (Left column) total gas (mobile + trapped CO_2) saturation at the end of injection; (middle column) total gas saturation at the end of monitoring; (right column) dissolved CO_2 (mole fraction) in brine at the end of monitoring. Arrow points North.

Compared to shallow drinking water aquifers, where often a certain amount of drilling, logging, and well test data exist, most deep saline aquifers proposed for GCS are extremely data-poor. At the FutureGen site, for example, only a few boreholes exist, similar to this study where the few existing measurements came from hydrocarbon exploration. In GCS, besides the needs to keep the cost of drilling down, we additionally wish to minimize the number of wells drilled so as to reduce the leakage risk. Thus, despite the knowledge that subsurface saline aquifers are heterogeneous (e.g., such as that can be gained from outcrop analogs or wireline logging at test holes), modelers often choose to either ignore smaller scale heterogeneity in building GCS site models, or choose simplified models. This assumption is often necessary because CO_2 simulation with a multiphase compositional simulator is computationally demanding when the simulation domain is large and when the prediction times extend to hundreds to thousands of years. However, insights of this study suggest that, when conducting uncertainty analysis, conceptual model assumption should be carefully evaluated using alternative models in addition to evaluating parameter uncertainty.

Finally, this work obtains a set of site-specific insights. The study method, when repeated for a different reservoir, will likely yield different results. For example, Zhang et al. (2014) modeled a deep inclined aquifer following a similar approach of developing multiple conceptual models. Because of significant formation dip, however, modeling choice was found to exert a much stronger influence on the predicted CO_2 storage. A runaway plume was indeed simulated, whereas $scCO_2$ continuously migrates along dip, thus different large-scale heterogeneities (as represented by the different conceptual models) are continuously experienced by the plume, which influences its trapping and storage. In this work, because of the lack of significant dip at the model site, gas plume is mostly aggregating near the injector. Therefore, whether or not the insights of this study can be extended to other saline aquifer sites will require additional research examining diverse systems, i.e., flat versus inclined, strongly versus weakly heterogeneous, porous versus fractured, nonreactive systems versus strongly reactive, shallow versus deep injection, sluggish versus strong background groundwater flow, etc.

6. Conclusion

Injection of supercritical CO_2 into deep saline aquifers is considered a promising option to mitigate climate change. To evaluate

a storage site, reservoir simulation is commonly performed with a geologic site model. This study conducts an uncertainty analysis of CO_2 storage in the Nugget Sandstone, a deep saline aquifer in western Wyoming with a large storage potential. Along with engineering and environmental parameters, conceptual model uncertainty and the associated impact on simulating CO_2 flow and storage is evaluated. For the Nugget Sandstone, using subsets of the available site data, a suite of increasingly complex geologic model families are built: a homogeneous model family (FAM1), a stationary petrophysical model family (FAM2), a stationary facies model family with sub-facies petrophysical variability (FAM3), and a non-stationary facies model family (with sub-facies variability) conditioned to soft data (FAM4). These families, representing alternative conceptual models built with increasing data, were simulated with the same CO_2 injection test (50 years at 1/10 Mt per year [1.0×108 kg/year]), followed by 2950 years of monitoring. Using design of experiment, an efficient sensitivity analysis is conducted for all families, systematically varying the uncertain input parameters, while assuming identical well configuration, injection rate, BHP constraint, and boundary conditions, i.e., model is considered part of a larger semi-infinite system, where both the injected CO_2 and the formation brine can flow out. For each family, parameter importance and prediction uncertainty are assessed over increasing times.

The sensitivity analysis outcomes are compared among the model families to identify parameters that have 1st order impact on predicting the CO_2 storage ratio (SR), at both time scales. For this deep aquifer with a gentle incline, geologic modeling choices do not significantly influence the short-term prediction of the storage ratio. However, geologic factors can become more important over longer times, but only for those families where such factors are accounted for (in other words, their long-term importance cannot be revealed by the relatively simple conceptual models). Based on results of the sensitivity study, a response surface (RS) analysis is conducted to generate prediction envelopes of the storage ratio, which are also compared among the families. Results suggest a large uncertainty in the predicted storage ratio, given the uncertainties in model parameters and modeling choices. At the end of injection, the SR varies from 5% to 60%; at the end of monitoring, it varies from 18% to 100%. The SR variation among the model families, however, is relatively small. At the proposed injection site, for the engineering and geologic uncertainty factors identified, long-term leakage risk is considered small. This is because, in the lowest-SR scenarios, all families predict gravity-stable $scCO_2$ that migrates toward the bottom of the reservoir. In the highest-SR scenarios, $scCO_2$ footprints are relatively insignificant by the end of monitoring due to significant dissolution. These results, though significant, depend on whether the EOS adopted by the reservoir simulator can correctly model the mixture densities.

The issue of conceptual model uncertainty is not limited to GCS modeling. This study is applicable to analyzing other subsurface data-poor environments, where key performance metrics can be evaluated against different conceptual models, and over time. For example, in Milliken et al. (2007), multiple reservoir models were evaluated as part of a screening analysis to understand whether complex site geology has an effect on oil recovery predictions. These reservoir models were built and simulated prior to when a single borehole was drilled. The multiple conceptual modeling approach can reveal insights that are difficult to discern with a single model. It is the most useful when it asks us this question: will conceptual model uncertainty, which varies with data support and our experience, skills, and perception of the site geology, affect the uncertainty outcomes – including important parameters and prediction uncertainty?

Acknowledgments

Funding for this study is provided by the Center for Fundamental of Subsurface Flow, School of Energy Resources, University of Wyoming. Partial funding is provided by NSF grant EAR-0838250. We acknowledge the generous donation of software (Petrel, Petrophysics Interactive, Eclipse) from Schlumberger, Inc. We acknowledge the thoughtful comments from two anonymous reviewers and the editor-in-chief, which have helped improve the organization and clarity of this paper.

References

Amudo, C., Graf, T., Harris, N.R., Dandekar, R., Amor, F.B., May, R.S., 2008. Experimental design and response surface models as a basis for stochastic history match – a Niger delta experience. In: IPTC, Paper was prepared for presentation at the International Petroleum Technology Conference, Kuala Lumpur, Malaysia, 3–5 December.

Bachu, S., 2000. Sequestration of CO_2 in geological media: criteria and approach for site selection in response to climate change. Energy Conversion and Management 41, 953–970.

Beni, A.N., Clauser, C., Erlstrom, M., 2011. System analysis of underground CO_2 storage by numerical modeling for a case study in Malmo. American Journal of Science 311, 335–368, http://dx.doi.org/10.2475/04.2011.03.

Birkholzer, J.T., Zhou, Q., 2009. Technical Report: Basin-Scale Hydrologic Impacts of CO_2 Storage: Regulatory and Capacity Implications.

Bourbiaux, B., 2010. Fractured reservoir simulation: a challenging and rewarding issue. Oil and Gas Science and Technology 65, 227–238.

Castellini, A., Chawathe, A., Larue, D., Landa, J.L., Jian, F.X., Toldi, J.L., 2003. What is relevant to flow? A comprehensive study using a shallow marine reservoir. In: SPE, Paper prepared for presentation at the SPE Reservoir Simulation Symposium, Houston, TX, 3–5 February.

Choi, K., Jackson, M., Hampson, G., Jones, A., Reynolds, T., 2007. Impact of heterogeneity on flow in fluvial-deltaic reservoirs: implications for the giant ACG field, south Caspian basin. In: SPE, Paper was prepared for presentation at the SPE Europec/EAGE Annual Conference and Exhibition, London, UK, 11–14 June.

David, W., Sacrison, W., Hanson, R., 1975. Structure history of Southwestern Wyoming as evidenced from outcrop and seismic. In: Dudley, W.B. (Ed.), Symposium on deep drilling frontiers in the central Rocky Mountains. , pp. 9–20, seismic cross section: A–A′ along Moxa Arch from south to north; B–B′ from west to east over Moxa Arch.

Deng, H., Stauffer, P.H., Dai, Z., Jiao, Z., Surdam, R.C., 2012. Simulation of industrial-scale CO_2 storage: multi-scale heterogeneity and its impacts on storage capacity, injectivity and leakage. International Journal of Greenhouse Gas Control 10, 397–418.

Easley, M., White, K., Freeman, B., Shafer, J.M., Sparks, D., 2013. Wyoming Infrastructure Authority (WIA) Summary of Activities, Report to Stakeholders Dated June 6.

Firoozabadi, A., Cheng, P., 2010. Prospects for subsurface CO_2 sequestration. American Institute of Chemical Engineers Journal 56, 1398–1405.

Forooghi, A., Hamouda, A.A., Eilertsen, T., 2009. Co-optimization of CO_2 EOR and sequestration in a north sea chalk reservoir. In: SPE, Paper was prepared for presentation at the 2009 SPE/EAGE Reservoir Characterization and Simulation Conference, Abu Dhabi, UAE, 19–21 October.

Friedmann, F., Chawathe, A., Larue, D.K., 2003. Assessing Uncertainty in Channelized Reservoirs Using Experimental Design. SPE Reservoir Evaluation and Engineering, pp. 264–274.

Ghomian, Y., Pope, G.A., Sepehrnoori, K., 2008. Hysteresis and field-scale optimization of wag injection for coupled CO_2-EOR and sequestration. In: SPE, Paper was prepared for presentation at the 2008 SPE/DOE Improved Oil Recovery Symposium, Tulsa, Oklahoma, 19–23 April.

Ghomian, Y., Sepehrnoori, K., Pope, G.A., 2010. Efficient investigation of uncertainties in flood design parameters for coupled CO_2 sequestration and enhanced oil recovery. In: SPE, Paper was prepared for presentation at the SPE International Conference on CO_2 Capture, Storage, and Utilization, New Orleans, LA, 10–12 November.

Harstad, H., Teufel, L., Lorenz, J., Brown, S., 1996. Characterization and Fluid Flow Simulation of Naturally Fractured Frontier Sandstone, Green River Basin, Wyoming. Sandia National Lab.

Huang, N.S., Aho, G.E., Baker, H.B., Matthews, T.R., Pottorf, R.J., 2011. Integrated reservoir modeling of a large sour-gas field with high concentrations of inerts. SPE Reservoir Evaluation and Engineering 41, Paper number 146082.

IPCC, 2013. Carbon dioxide capture and storage. In: Underground Geological Storage (Chapter 5) http://www.ipcc.ch/search/searchspecialreports.shtml

Jian, F.X., Larue, D.K., Toldi, A.J., 2002. Reservoir modeling methods and characterization parameters for a shoreface reservoir: what is important for fluid flow performance? SPE.

Larue, D.K., Friedmann, F., 2001. Stratigraphic uncertainty in field development studies: a conceptual modeling approach. The Leading Edge 20 (January), 28–33.

Li, B., Friedmann, F., 2005. A novel response surface methodology based on "amplitude factor" analysis for modeling nonlinear responses caused by both reservoir

and controllable factors. In: SPE, Paper was prepared for presentation at the 2005 SPE Annual Technical Conference and Exhibition, Dallas, TX, 9–12 October.
Li, B., Friedmann, F., 2006. Semiautomatic multiple resolution design for history matching. In: SPE, Paper was prepared for presentation at the (2006) SPE Annual Technical Conference and Exhibition, San Antonio, TX, 24–27 September.
Li, H., White, C.D., 2003. Geostatistical models for shales in distributary channel point bars (Ferron sandstone, Utah): from ground-penetrating radar data to three-dimensional flow modeling. AAPG Bulletin 87, 1851–1868.
Li, S.Q., Zhang, Y., Zhang, X., 2011. Geologic modeling and fluid-flow simulation of acid gas disposal in western Wyoming. AAPG Bulletin 96, 635–664.
Liu, B., Zhang, Y., 2011. CO_2 modeling in a deep saline aquifer: a predictive uncertainty analysis using design of experiment. Environmental Science and Technology 45, 3504–3510, http://dx.doi.org/10.1021/es103187b.
Liu, B., Zhang, Y., Zhang, X., 2011. Acid gas storage in a deep saline aquifer: a numerical sensitivity study on parameter and model uncertainty. Journal of Hazardous, Toxic and Radioactive Waste 15, http://dx.doi.org/10.1061/(ASCE)HZ.1944-8376.0000061.
Lu, C., Han, W.S., McPherson, B.J., Lichtner, P.C., 2009. Effects of density and mutual solubility of a CO_2-brine system on CO_2 storage in geological formations: "warm" vs. "cold" formations. Advances in Water Resources 32, 1685–1702, http://dx.doi.org/10.1016/j.advwaters.2009.07.008.
Ma, Y.Z., Seto, A., Gomez, E., 2009. Depositional facies analysis and modeling of the Judy creek reef complex of the upper Devonian swan hills, Alberta, Canada. AAPG Bulletin 93, 1235–1256.
Meddaugh, W.S., Griest, S.D., Gross, S.J., 2004. Application of design of experiments to expedite probabilistic assessment of reservoir hydrocarbon volumes (OOIP). In: Geostatistics Banff., pp. 751–756.
Milliken, W.J., Levy, M., Strebelle, S., Zhang, Y., 2007. The effect of geologic parameters and uncertainties on subsurface flow: deepwater depositional systems. In: SPE, Paper was prepared for presentation at the 2007 SPE Annual Technical Conference and Exhibition, Anaheim, CA, 11–14 November.
Montgomery, D.C., 2008. Design and Analysis of Experiments, 7th ed. John Wiley & Sons, Inc, ISBN number: 978-0-470-39882-1.
Mosse, Y., Portier, E., Schaaf, T., 2010. CCS project in a gas field of the Sbaa basin, SW Algeria – what is at stake? In: SPE, Paper was prepared for presentation at the SPE North Africa Technical Conference and Exhibition, Cairo, Egypt, 14–17 February.
Myers, R., Montgomery, D., 1995. Response Surface Methodology – Process and Product Optimization Using Designed Experiments. John Wiley & Sons, New York.
Narahara, G.M., Spokes, J.J., Brennan, D.D., Maxwell, G., Bast, M., 2004. Well count optimization incoporating a wide range of uncertainties for the deepwater Agbami field. In: SPE, Paper was prepared for presentation at the Offshore Technology Conference, Houston, TX, 3–6 May.
O'Dell, P.M., Lindsey, K.C., 2010. Uncertainty management in a major CO_2 EOR project. In: SPE, Paper was prepared for presentation at the Abu Dhabi International Petroleum Exhibition and Conference, Abu Dhabi, UAE, 1–4 November.
Peng, C.Y., Gupta, R., 2004. Experimental design and analysis methods in multiple deterministic modeling for quantifying hydrocarbon in-place probability distribution curve. In: SPE, Proceedings: Asia Pacific Conference on Integrated Modelling for Asset Management, Kuala Lumpur, Malaysia, 29–30 March.
Purwar, S., Jablonowski, C.J., Nguyen, Q.P., 2010. A method for integrating response surfaces into optimization models with real options: a case study in gas flooding. In: SPE, Paper was prepared for presentation at the SPE Hydrocarbon Economics and Evaluation Symposium, Dallas, TX, 8–9 March.
Razavi, S., Tolson, B.A., Burn, D.H., 2012. Review of surrogate modeling in water resources. Water Resources Research 48 (W07), 401, http://dx.doi.org/10.1029/2011WR011527.
Royse, F., Warner, M., Reese, D., 1975. Thrust Belt Structure Geometry and Related Stratigraphic problems: Wyoming, Idaho, northern Utah. In: Bolyar, D.W. (Ed.), Symposium on deep drilling frontiers in the central Rocky Mountains. , pp. 41–54, seismic cross section Plat III (Right).
Salhi, M.S.A., Rijen, M.F.V., Alias, Z.A., Visser, F., Dijk, H., Lee, H.M., Timmerman, R.H., Upadhyaya, A.A., Wei, L., 2005. Reservoir modeling for redevelopment of a giant fractured carbonate field, Oman: experimental design for uncertainty management and production forecasting. In: SPE, Paper was prepared for presentation at the International Petroleum Technology Conference, Doha, Qatar, 21–23 November.
Schlumberger, 2009a. ECLIPSE Technical Manual: The GASWAT Option.
Schlumberger, 2009b. Petrel User's Manual.
Sifuentes, W., Blunt, M.J., Giddins, M.A., 2009. Modeling CO_2 storage in aquifers: assessing the key contributors to uncertainty. In: SPE, Paper was prepared for presentation at the 2009 SPE Offshore Europe Oil and Gas Conference and Exhibition, Aberdeen, UK, 8–11 September.
Stauffer, P., Surdam, R., Jiao, Z., Miller, T.A., Bentley, R.D., 2009a. Combining geologic data and numerical modeling to improve estimates of the CO_2 sequestration potential of the rock springs uplift, Wyoming. Energy Procedia 1, 2717–2724.
Stauffer, P., Viswanathan, H., Pawar, R., Guthrie, G., 2009b. A system model for geologic sequestration of carbon dioxide. Environmental Science and Technology 43, 565–570.
Wang, F., White, C.D., 2002. Designed simulation for a detailed 3D turbidite reservoir model. In: SPE, Paper was prepared for presentation at the SPE Gas Technology Symposium, Calgary, Alberta, Canada, 30 April–2 May.
White, C.D., Willis, B.J., Narayanan, K., Dutton, S.P., 2001. Identifying and estimating significant geologic parameters with experimental design. SPE Journal 6, 311–324.
Wood, K.J., Lake, L.W., Johns, R.T., Nunez, V., 2008. A Screening Model for CO_2 Flooding and Storage in Gulf Coast Reservoirs Based on Dimensionless Groups. SPE Reservoir Evaluation and Engineering, pp. 513–520.
Ye, M., Cooper, C.A., Chapman, J.B., Gillespie, D., Zhang, Y., 2009. A geologically based Markov chain model for simulating tritium transport with uncertain conditions in a nuclear-stimulated natural gas reservoir. SPE Reservoir Evaluation & Engineering 12, 974–984, http://dx.doi.org/10.2118/114920-PA, SPE-114920-PA.
Ye, M., Pohlmann, K.F., Chapman, J.B., Pohll, G.M., Reeves, D.M., 2010. A model-averaging method for assessing groundwater conceptual model uncertainty. Ground Water, http://dx.doi.org/10.1111/j.1745-6584.2009.00633.x.
Yeten, B., Castellini, A., Guyaguler, B., Chen, W.H., 2005. A comparison study on experimental design and response surface methodologies. In: SPE, Paper was prepared for presentation at the 2005 SPE Reservoir Simulation Symposium, Houston, TX, 31 January–2 February.
Zabalza-Mezghani, I., Manceau, E., Feraille, M., Jourdan, A., 2004. Uncertainty management: from geological scenarios to production scheme optimization. Journal of Petroleum Science and Engineering 44, 11–25.
Zhang, J., Delshad, M., Sepehrnoori, K., 2007. Development of a framework for optimization of reservoir simulation studies. Journal of Petroleum Science and Engineering 59, 135–146.
Zhang, Y., Yang, G., Li, S.-Q., 2014. Uncertainty analysis of modeling carbon sequestration in a deep inclined saline aquifer. Journal of Hazardous, Toxic, and Radioactive Waste (in review).